M.Sc. Thesis

Interference cancellation techniques for low power wireless sensors

Venkatasubramanian Sridharan
Student number: 4118154

Abstract

Non-coherent on-off keying (OOK) receivers are preferred in ultra low power (ULP) wireless devices as they consume less power when compared to receivers based on other modulation schemes. However, these devices are highly susceptible to co-channel interference (CCI). Therefore, interference cancellation (IC) techniques for ULP non-coherent OOK receivers are investigated in this thesis.

Various IC techniques are discussed in literature. However, the non-coherent OOK receiver architecture calls for the design of new low complexity IC techniques. The main constraint of the system is imposed by the analog front end that uses a simple square law detector to down-convert the RF signals to baseband and there is also only single radio frequency (RF) chain. The challenge is to mitigate CCI under these constraints and improve the detection performance.

The non-coherent detection of OOK signals requires the knowledge of the signal to noise ratio (SNR) of the incoming signal. Therefore, SNR estimation plays an important role in non-coherent OOK receivers. Thus the scope of this thesis is twofold. Firstly, the SNR estimation and non-coherent detection techniques are proposed for OOK signals. Secondly, the interference mitigation techniques are proposed for the case of continuous wave (CW) CCI and OOK modulated interferers. The problems of the proposed techniques for the case of M-ary phase shift keying (MPSK) modulated interferers are also investigated. Finally, the implementation of the SNR estimation techniques on real time hardware platform is discussed.

Faculty of Electrical Engineering, Mathematics and Computer Science
Delft University of Technology

Interference cancellation techniques for low power wireless sensors

Thesis

submitted in partial fulfillment of the
requirements for the degree of

Master of Science

in

Electrical Engineering

by

Venkatasubramanian Sridharan
born in Tirunelveli, India

This work was performed in:

Wireless Group,
Holst Centre/Imec,
Hightech Campus 31,
5656 AE, Eindhoven, The Netherlands.

Delft University of Technology
Department of
Telecommunications

The undersigned hereby certify that they have read and recommend to the Faculty of Electrical Engineering, Mathematics and Computer Science for acceptance a thesis entitled **"Interference cancellation techniques for low power wireless sensors"** by **Venkatasubramanian Sridharan** in partial fulfillment of the requirements for the degree of **Master of Science**.

Dated: 20-June-2012

Chairman: ______________________

Prof. Dr. O. Yarovoy

Advisors: ______________________

Dr. H. Nikookar

____

Dr. N. F. Kiyani

Committee Members: ______________________

Dr. Ir. M. J. Bentum

Acknowledgements

First of all, I would like to thank my supervisor Dr. Nauman. F. Kiyani for providing me the opportunity to do this work at Holst Centre/Imec. Thank you Nauman for your invaluable guidance, highly constructive technical discussions, positive attitude, patience and constructive criticisms. More than the technical aspects, I have learnt the value of perseverence and patience from you. It was a great opportunity to work with you and I hope our association continues in future paving way for many more technical contributions.

I would like to thank my supervisor, Dr. Homayoun Nikookar for his timely support, positive attitude, patience and valuable comments. Thank you Homayoun for being a constant source of encouragement that has helped me a lot to make effective contributions in this thesis. It was a great opportunity to work with you. Thank you once again for being a pleasant supervisor to work with and I hope our association continues in future paving way for many more technical contributions.

I would like to thank Prof. Dr. Olexander Yarovoy and Dr. Ir. Mark Bentum for allocating their time and expressing their interest to review this work.

I would like to thank my colleagues at Imec for providing their technical suggestions which helped me to enhance the contributions of this thesis.

I would also like to thank all my friends for being a constant source of encouragement throughout my thesis work.

Finally, I would like to thank my parents, sister and relatives for their constant support and encouragement.

Venkatasubramanian Sridharan
Delft, The Netherlands
20-June-2012

Contents

List of Figures

List of Tables

Abbreviations

ADC	Analog to Digital Converter
AWGN	Additive White Gaussian Noise
BAN	Body Area Network
BER	Bit Error Rate
CCI	Co-Channel Interference
CDMA	Code Division Multiple Access
CRLB	Cramer-Rao Lower Bound
CW	Continuous Wave
DA	Data Aided
DDC	Digital Down Converter
DOA	Direction of Arrival
EM	Expectation Maximization
FDMA	Frequency Division Multiple Access
IC	Interference Cancellation
ISI	Inter Symbol Interference
LMS	Least Mean Square
MAI	Multiple Access Interference
MAP	Maximum-A-Posteriori
MFSK	M-ary Frequency Shift Keying
ML	Maximum Likelihood
MPSK	M-ary Phase Shift Keying
MQAM	M-ary Quadrature Amplitude Modulation
$\mathbf{M_1}$	First Moment
$\mathbf{M_2}$	Second Moment
$\mathbf{M_3}$	Third Moment
NCRLB	Normalized Cramer-Rao Lower Bound
NDA	Non Data Aided
NML	Normalized Max-Zero Likelihood
NMSE	Normalized Mean Square Error
OOK	On-Off Keying
PDF	Probability Density Function
PIC	Parallel Interference Cancellation
PSK	Phase Shift Keying
RF	Radio Frequency
RFID	Radio Frequency Identification
RLS	Recursive Least Square
SIC	Successive Interference Cancellation
SINR	Signal to Interference plus Noise Ratio
SNR	Signal to Noise Ratio
TDMA	Time Division Multiple Access
ULP	Ultra Low Power
USRP2	Universal Software Radio Peripheral 2

1 Introduction

1.1 Introduction to wakeup radio

In recent years, there has been a growing interest in the development of energy efficient ultra low power (ULP) wireless devices for various applications, for instance, wireless sensor networks, active RFID, short range communications and body area networks (BAN) for healthcare. The main feature of the wireless devices used in these applications is long life time through energy efficient operation.

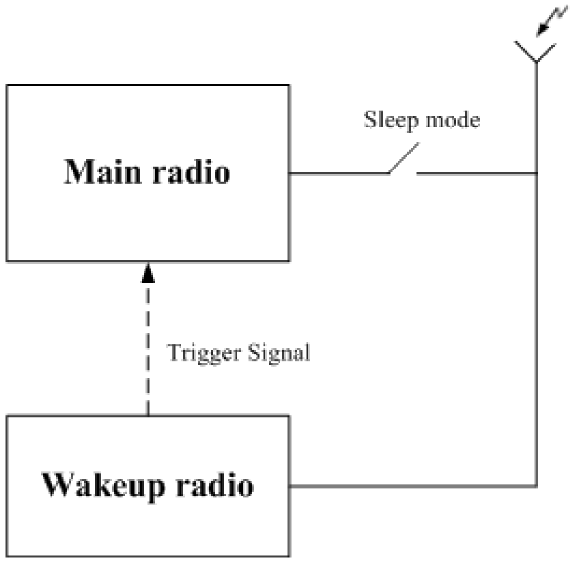

Figure 1.1: Operation of the dual radio system equipped with a wakeup radio and main radio.

Recently, the concept of a wakeup radio is introduced to improve the energy efficiency of low power radio, e.g., [1,2], and the references therein. The wakeup radio is an ULP wireless receiver which is used in conjunction with a high performance main radio as shown in figure 1.1. The design of this dual radio system is motivated by the fact that the main radio need not be always on. The main radio is assigned a specific address and it follows a sleep/active mode cycle. More specifically, the low power wakeup radio is always in the listening mode and triggers the main radio if the packet is addressed to the main radio. The main radio returns to sleep mode after the communication ends. Thus the wakeup radio assists the main radio in low power channel monitoring and to operate in a near zero standby power when the main radio is in the sleep state. Figure 1.2 depicts the sleep mode/active mode cycle of the main radio. It is evident that, the power consumption is reduced as the main radio is not always on. Though the ULP wakeup radio improves the energy efficiency, it is highly susceptible to interference.

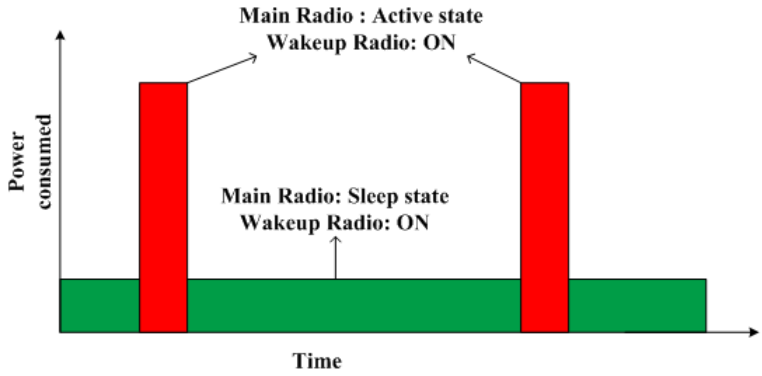

Figure 1.2: Operation cycle of the main radio and wakeup radio.

Hence, interference mitigation in the wakeup radio is an important aspect of research. In this chapter, we define the interference mitigation problem and explain the need for novel interference mitigation techniques for the wakeup radio.

The rest of this chapter is organized as follows. Section 1.2 gives an overview on the types of interference. Section 1.3 briefly describes the existing interference cancellation techniques. The interference issues in the wakeup radio and the problem formulation of the thesis are described in section 1.4. Section 1.5 gives a brief outline on the contributions of rest of the chapters of this thesis.

1.2 Types of interference

Interference can be broadly classified into the following types based on the relation of the interfering signal to the desired signal.

- Inter symbol interference
- Co-channel interference
- Multiple access interference

These types of interference are described in the following subsections.

1.2.1 Inter symbol interference (ISI)

ISI occurs due to the non flat frequency response of the channel which results in time dispersion of the signals. The transmitted pulse is spread and has a greater duration when it is distorted due to time dispersion. This causes the overlap of the stream of pulses at the receiver. The ISI is usually mitigated by employing appropriate pulse shaping. The spectral characteristic ($G(f)$) of the pulse should follow the Nyquist criterion for zero ISI which is given by, [4]

$$\sum_{m=-\infty}^{\infty} G(f + \frac{m}{T}) = T. \tag{1.1}$$

where, f is the frequency and T is the time duration of the pulse. The widely used pulse shape in practice is the raised cosine pulse shape which satisfies the Nyquist criterion for zero ISI. Usually, the raised cosine frequency response is split between the transmitter and receiver. A root raised cosine pulse is used in the transmitter side and a similar root raised cosine pulse is used as a matched filter in the receiver to give the overall raised cosine frequency response. The pulse shape ($g(t)$) of the root raised cosine pulse is given by,

$$g(t) = \begin{cases} \frac{1}{\sqrt{T}} \frac{4\lambda t/T \cos\left[(1+\lambda)\pi t/T\right] + \sin\left[(1-\lambda)\pi t/T\right]}{(\pi t/T)(1-(4\lambda t/T)^2)}, & \text{if } t \neq 0, t \neq \pm\frac{T}{4\lambda}, \\ \frac{1}{\sqrt{T}}(1 - \lambda + (4\lambda/\pi)) & \text{if } t = 0, \\ \frac{\lambda}{\sqrt{2T}}\left[(1 + 2/\pi)\sin(\pi/4\lambda) + (1 - 2/\pi)\cos(\pi/4\lambda)\right] & \text{if } t = \pm\frac{T}{4\lambda}. \end{cases} \tag{1.2}$$

where, λ is the roll off factor ($0 \leq \lambda \leq 1$). Figure 1.3 shows a root raised cosine pulse shape with roll off factor $\lambda = 0.5$

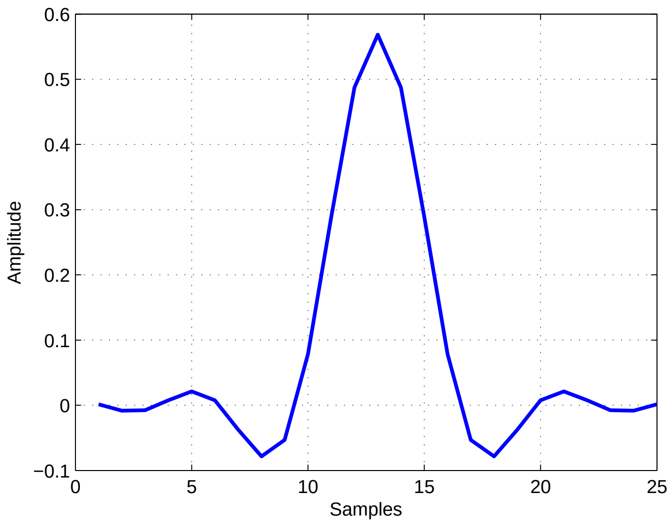

Figure 1.3: Root raised cosine pulse shape.

1.2.2 Co-channel interference (CCI)

CCI occurs when two or more signals overlap in frequency domain. CCI is detrimental to the receiver detection performance and this thesis primarily deals with the CCI interference mitigation techniques for the wakeup radio receiver. CCI can be broadly subdivided into the following types.

Continuous wave (CW) interferer
Continuous wave interferer is one whose bandwidth is less than the desired signal bandwidth. It is a continuous sinusoid around the center frequency of the desired signal.

Modulated interferer

The interference due to the modulated interferer is caused when the bandwidth of the desired signal overlaps with the bandwidth of the modulated signal from another source. The modulated interferer can occupy the entire spectrum of desired signal or occupy a part of it depending on the center frequency and data rate of the interfering source.

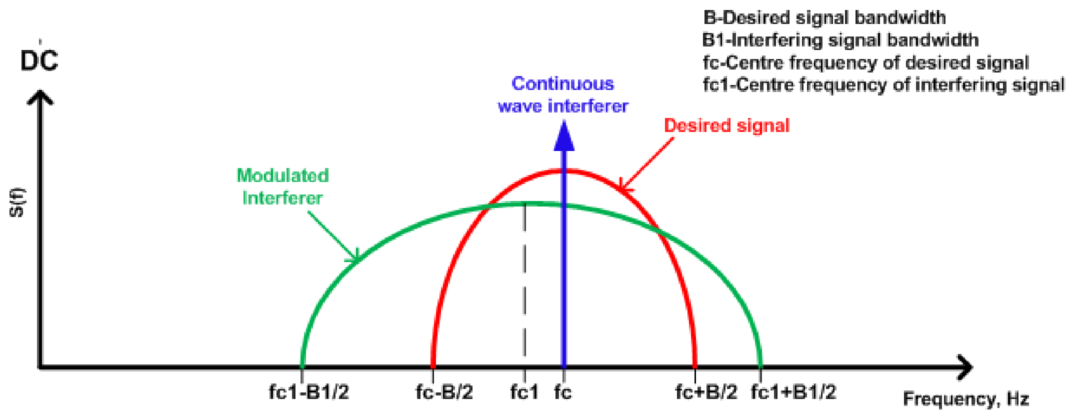

Figure 1.4: Spectrum of the different types of co-channel interferers and the desired signal.

Figure 1.4 shows the spectrum ($S(f)$) of different kind of CCI signals along with the desired signal. The modulated interferer in the figure is shown to be overlapping the entire spectrum of the desired signal just for illustration purpose. It can overlap only with a part of the desired signal's spectrum as well.

1.2.3 Multiple access interference (MAI)

MAI occurs usually in cellular communication systems when two or more signals share the same bandwidth. MAI can be eliminated if the signals are orthogonal. The orthogonality can be achieved by time division multiple access (TDMA), frequency division multiple access (FDMA) or code division multiple access (CDMA) techniques. In TDMA systems, each user is assigned different time slots for transmission and reception. In FDMA systems, each user is assigned a specific band of non overlapping frequencies. In case of CDMA systems, the signals of each user are spread by a specific code sequence and the codes are orthogonal to each other. Thus the receiver is able to decode each user's signal after correlating the multiplexed incoming signal with the appropriate code sequence. MAI can still occur in CDMA systems since ideal time synchronisation is not present between the users which leads to non-orthogonal signals. Multipath also contributes to MAI.

In the following section, we present a brief overview on some of the existing interference cancellation techniques discussed in the literature.

1.3 Types of interference cancellation techniques

There are number of interference cancellation techniques discussed in the literature. Most of these techniques fall under the following categories.

- Filter based approach
- Spatial processing
- Joint/multiuser detection

1.3.1 Filter based methods

Filter based techniques generate the frequency response function such that it maximizes the signal to interference plus noise ratio (SINR) at the output of the filter. The optimal filter that maximizes the SINR is the Wiener filter, [5]. The weight matrix (W) of the Wiener filter is given by,

$$\begin{aligned} W &= R_x^{-1} R_{xs}, \\ R_x &= \frac{1}{N} X X^H, \\ R_{xs} &= \frac{1}{N} X S^H. \end{aligned} \tag{1.3}$$

where, R_x, is the M x M data covariance matrix and R_{xs} is M x 1 correlation matrix between the data and source symbols, X is the M x N received sample data matrix and S is the 1 x N vector of corresponding source symbols, M and $N$are the number of antennas and data samples, respectively. W can be obtained through a set of training sequences. To avoid the computation of the inverse of the covariance matrix, adaptive algorithms such as least mean square (LMS) and recursive least square (RLS) shall be used, [6]. Generally, the filter based techniques are suitable to remove narrowband interference.

1.3.2 Spatial processing

The spatial processing techniques require multiple antennas at the receiver. Interference cancellation can be performed by multiple antenna techniques such as beamforming. In case of beamforming, the spatial diversity is exploited. If the interfering signals are spatially separated, then the receiving antenna array can be steered towards the direction of source signal. Various spatial processing techniques have been proposed in literature to cancel interference by source separation [7].

1.3.3 Joint/multiuser detection

Joint or multiuser detection is required if there are multiple signals with the same characteristics. In that case, a signature is added to each signal such that it can be detected in the presence of other signals. For example, in the case of CDMA, the signals of each user are spread by a specific code sequence and the codes are orthogonal to each other. Thus the receiver is able to decode each user's signal after correlating the multiplexed incoming signal with the appropriate code sequence. When the orthogonality of the codes are disturbed, cross correlation exists between the multiple signals. In that case, advanced techniques such as successive interference cancellation (SIC) and parallel interference cancellation (PIC) are used, [8, 9].

In the case of wakeup radio, there are system constraints. Due to the constraints, the above techniques cannot be used in the wakeup radio receiver. These are explained in detail in chapter 3. In the following section, the problem formulation of this thesis is described in detail.

1.4 Problem formulation

The wakeup radio employs a non-coherent on-off keying (OOK) receiver architecture. OOK is used as the modulation scheme as it helps to reduce the power consumption. The non-coherent receiver uses a square law detector and a low pass filter to downconvert the radio frequency (RF) signal to baseband and does not require a local oscillator which further helps to reduce power consumption. Though the architecture of the wakeup radio is advantageous in terms of the reduced power consumption, it is highly susceptible to CCI. CCI mitigation is important to have an agreeable detection performance in the wakeup radio receiver. In this thesis, the following types of CCI are considered.

- Continuous wave interferer
- OOK modulated interferer
- M-ary phase shift keying (MPSK) modulated interferer

It is also important to know that the detection threshold is a function of received signal to noise ratio (SNR) in the case of non-coherent OOK receiver, [3]. Hence, SNR estimation has to be done in the receiver for non-coherent detection of OOK signals. Therefore, in this thesis, SNR estimation and interference mitigation techniques for non-coherent OOK receivers are investigated in detail.

The main contributions of the rest of the chapters of this thesis are highlighted in the following section.

1.5 Thesis contributions

Chapter 2: SNR estimation and non-coherent detection techniques for OOK signals

At first, we propose a novel normalized max-zero likelihood (NML) technique for non-coherent detection of OOK signals. Then, moments based M_1V estimator and maximum likelihood (ML) estimator are proposed for data aided (DA) SNR estimation. Then, expectation maximization (EM), M_1M_2 and M_2M_3 estimators are proposed for non data aided (NDA) SNR estimation. The normalized mean square error (NMSE) performance of each estimator is evaluated over a wide range of SNR and the limitations of the estimators are discussed. Hybrid $M_1M_2 - EM$ and $M_2M_3 - EM$ estimators are proposed to overcome the limitations. Finally, the bit error rate (BER) performance of the DA and hybrid NDA estimators is simulated and is found to be in good agreement with the analytically evaluated BER.

Chapter 3: Interference mitigation techniques for wakeup radio
DA and NDA estimation techniques proposed in chapter 2 are extended to estimate the interference power along with the desired signal and noise power. Based on these estimates, threshold based and maximum-a-posteriori (MAP) detector based interference mitigation techniques are proposed for the case of CW and OOK modulated interferers. BER performance of these techniques is evaluated and compared against the theoretical BER. Finally, the limitations of these techniques are discussed.

Chapter 4: Implementation of non data aided SNR estimation
The implementation of NDA SNR estimation techniques in universal software radio peripheral 2 (USRP2) platform is described in detail. At first, the transmitter implementation using a combination of Tektronix function generator and signal generator is discussed. Then, the USRP2 receiver implementation is described in detail and the results of the implementation are discussed.

Chapter 5: Conclusions and future scope
The main contributions of this thesis are summarized and the possible directions for future work are highlighted in this chapter.

SNR estimation and non-coherent detection techniques for OOK signals

2

2.1 Introduction

Non-coherent on-off keying (OOK) receiver architecture is preferred for ultra low power (ULP) wakeup radio as OOK modulation and non-coherent detection leads to low power consumption. The non-coherent detection requires the knowledge of the signal to noise ratio (SNR) at the receiver. The knowledge of SNR is also important in other radios for practical applications, e.g, power control, scheduling, etc. Hence, in this chapter we discuss non-coherent detection and SNR estimation techniques for wakeup radio.

The conventional non-coherent detection of OOK signals is based on the comparison of the received baseband signal samples against a decision threshold [3]. The decision threshold is a function of signal-to-noise ratio (SNR) and it is approximated for high SNR, [3]. The bit error rate (BER) performance of the threshold based technique comes close to the maximum likelihood (ML) method when SNR increases. In this letter, we propose a novel normalized max-zero likelihood (NML) detection method for non-coherent detection of OOK signals which improves the BER performance when compared against the ML method and a maximum gain of 1 dB is achieved at 2×10^{-4} BER. Since, the threshold based, ML and NML techniques require the knowledge of SNR, SNR estimation techniques are investigated for non-coherent detection of OOK signals.

SNR estimation techniques can be broadly classified as data aided (DA) and non data aided (NDA) schemes. DA SNR estimation is carried out when the received data sequence is known at the receiver and NDA SNR estimation is carried out in the case of unknown received data sequence. Various SNR estimation techniques have been discussed in the literature, e.g., [12–16] and the references therein. DA SNR estimation for M-ary phase shift keying ($MPSK$) signals is proposed in [12]. The comparison of SNR estimation techniques in additive white Gaussian noise (AWGN) channel for $MPSK$ signal constellations is reported in [13]. NDA envelope detector based SNR estimators are proposed for M-ary quadrature amplitude modulation ($MQAM$) and PSK constellations in [14]. The expectation-maximization (EM) algorithm based SNR estimation for $MQAM$ signals is described in [15]. Maximum likelihood (ML) based DA and NDA SNR estimation techniques for non-coherent M-ary frequency shift keying ($MFSK$) receivers have been described in [16]. However, the existing SNR estimators, [12–16], are not suitable for non-coherent OOK receivers as they are characterized by the continuous availability of signal whereas, OOK signals are characterized by the presence and absence of the signal. Therefore, we propose novel SNR estimation techniques for non-coherent OOK receivers.

Moments based M_1V estimator and ML estimator are proposed for DA estimation. EM, M_1M_2 and M_2M_3 estimators are proposed for NDA SNR estimation. M_1, M_2 and M_3 are the first, second and third moments of the received baseband signal samples, respectively. M_1M_2 and M_2M_3 estimators are proposed for the condition of unequiprobable and equiprobable symbols, respectively.

Although the OOK signal is generally assumed to be composed of equiprobable symbols, it is quite important to consider the case of unequiprobable symbols in the context of ULP wireless devices. The unequiprobable symbol condition can occur when the source bits are mapped to codewords such that the codewords have few number of ones, resulting in reduced power consumption, [17]. It is shown further that, if the symbols are equiprobable, M_1M_2 estimator does not yield a solution for SNR estimate. It is also show that the performances of moments based estimators degrade in the high SNR region. EM estimator is proposed to overcome this problem. The normalized mean square error (NMSE) performance of each estimator is evaluated over a wide range of SNR and the limitations of the estimators are discussed. Hybrid $M_1M_2 - EM$ and $M_2M_3 - EM$ estimators are proposed to overcome the limitations. Finally, BER performance of the DA and hybrid NDA estimators is simulated and is found to be in good agreement with the analytically evaluated BER.

The rest of this chapter is organized as follows. Section 2.2 describes the system model. Section 2.3 describes the NML detection. DA SNR estimation is presented in section 2.4. Section 2.5 describes NDA SNR estimation. Section 2.6 describes the BER performance of the SNR estimators. Finally we summarize the findings of this chapter in section 2.7.

2.2 System model

The simplified model of OOK transmitter is shown in figure 2.1. The transmitted OOK

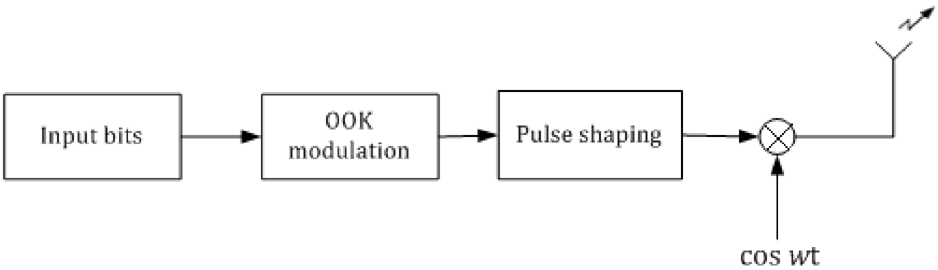

Figure 2.1: Simplified non-coherent OOK transmitter model.

signal ($s(t)$) is given by,

$$s(t) = \sum_{k=0}^{N-1} Ac_k g(t - (k-1)T)\cos(2\pi f_c t) \tag{2.1}$$

where, A is the amplitude of the signal, $c_k \in \{0, 1\}$ represent the transmitted OOK symbols, N is the total number of transmitted bits, $g(t)$ is the pulse shape, T is the bit duration and f_c is the centre frequency.

Assuming AWGN channel, the received RF signal ($r(t)$), is given by,

$$r(t) = s(t) + n(t) \tag{2.2}$$

where $n(t)$ is the zero mean complex Gaussian noise with noise variance σ^2 in each dimension.

Figure 2.2 shows the simplified model of the non-coherent OOK receiver. $r(t)$ is

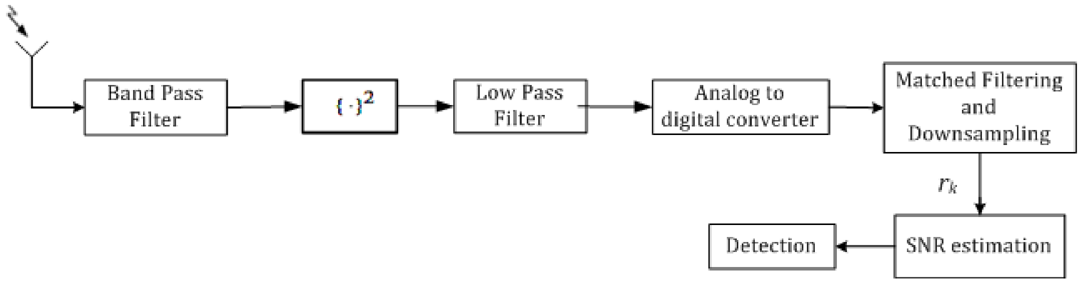

Figure 2.2: Simplified non-coherent OOK receiver model.

converted to baseband by a square law device and low pass filter. Assuming perfect synchronization, the received baseband signal (r_k) is given as,

$$r_k \quad = \quad (Ac_k + x_k)^2 + y_k^2, \qquad\qquad k = 0...N-1, \tag{2.3}$$

where, x_k and y_k are the real and imaginary parts of the complex Gaussian noise samples.

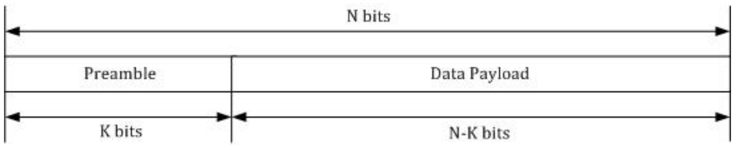

Figure 2.3: The data packet structure with K preamble bits and $N-K$ payload bits.

Consider the data packet structure as shown in figure 2.3. The total packet length is N bits, where the first K bits denote the preamble and the next $N-K$ bits comprise of the payload. Let $C_N = [c_0\ c_1\ ....\ c_{N-1}]^T$ represent the transmitted binary sequence. Let $C_K = [c_0\ c_1\ ....\ c_{K-1}]^T$ represent the transmitted binary sequence corresponding to the preamble and $C_K \Subset C_N$. Let $R_N = [r_0\ r_1\ ....\ r_{N-1}]^T$ represent the received baseband signal sequence. Let $R_K = [r_0\ r_1\ ....\ r_{K-1}]^T$ represent the received baseband signal sequence corresponding to the preamble and $R_K \Subset R_N$. The SNR (ρ) that has to be estimated from the received sequence is defined as,

$$\rho = \frac{A^2}{2\sigma^2}. \tag{2.4}$$

The bits are detected after SNR estimation. The distinction of Mark (transmission of binary 1) and Space (transmission of binary 0) is based on the comparison of r_k against a threshold (b_0). The conditional probability density functions (pdf) of r_k are given by [3].

$$p(r_k|c_k = 1) = \frac{1}{2\sigma^2} e^{-\frac{r_k + A^2}{2\sigma^2}} I_0\Big(\frac{\sqrt{r_k}A}{\sigma^2}\Big), \tag{2.5}$$

$$p(r_k|c_k = 0) = \frac{1}{2\sigma^2} e^{-\frac{r_k}{2\sigma^2}}, \tag{2.6}$$

where, $I_0(x)$ is the zeroth order modified Bessel function of the first kind. The probability of Mark error (P_m), Space error (P_s) and the overall probability of error (P_e) for equiprobale symbol conditions are given in [3] for envelope detector based receivers. They can be generalized for square law detector based receivers as follows.

$$\begin{aligned} P_m &= P(r_k <= b_0), \\ &= 1 - \int_{b_0}^{\infty} p(r_k|c_k = 1) \;\; dr_k, \\ &= 1 - \int_{b_0}^{\infty} \frac{1}{2\sigma^2} e^{-\frac{r_k + A^2}{2\sigma^2}} I_0\Big(\frac{\sqrt{r_k}A}{\sigma^2}\Big) \;\; dr_k. \end{aligned} \tag{2.7}$$

(2.7) can be simplified by applying the following transformations.

$$r_n^2 = \frac{r_k}{\sigma^2}, \tag{2.8}$$

$$\rho = \frac{A^2}{2\sigma^2}, \tag{2.9}$$

$$\beta = \frac{\sqrt{b_0}}{\sigma}. \tag{2.10}$$

Then,

$$\begin{aligned} P_m &= 1 - \int_{\beta}^{\infty} r_n e^{-\frac{r_n^2 + (\sqrt{2\rho})^2}{2}} I_0\Big(r_n \sqrt{2\rho}\Big) \;\; dr_n, \\ &= 1 - Q(\sqrt{2\rho}, \beta), \\ P_s &= \int_{b_0}^{\infty} p(r_k|c_k = 0) \;\; dr_k, \\ &= \int_{\beta}^{\infty} r_n e^{-\frac{r_n^2}{2}} \;\; dr_n, \\ &= e^{(-\frac{\beta^2}{2})}, \\ P_e &= \alpha P_m + (1 - \alpha) P_s, \end{aligned} \tag{2.11}$$

where, 'α' is the probability of '$c_k = 1$', '$1 - \alpha$' is the probability of '$c_k = 0$' and $Q(a, b)$ is the marcum Q function given by,

$$Q(a, b) = \int_b^{\infty} x e^{-(a^2 + x^2)/2} I_0(ax) \;\; dx.$$

The threshold b_0 is given by the intersection of $p(r_k|c_k = 1)$ and $p(r_k|c_k = 0)$ as shown in figure 2.4. Hence, for equiprobable symbol condition, the solution can be obtained

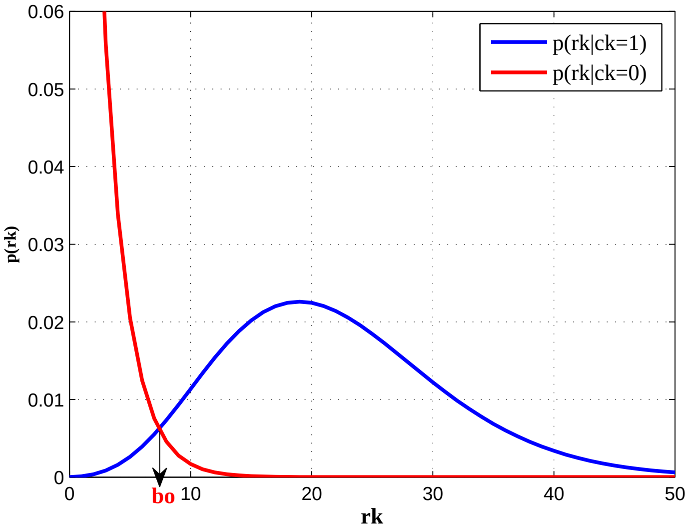

Figure 2.4: Pdfs for $c_k = 1$ and $c_k = 0$. SNR is assumed to be 10 dB. The optimal threshold b_0 is the intersection point of the pdfs

by equating $p(r_k|c_k = 1)$ and $p(r_k|c_k = 0)$ at the point $r_k = b_0$. To incorporate all probable symbol conditions, we have to equate,

$$\begin{aligned} \frac{\alpha}{2\sigma^2} e^{-\frac{b_0+A^2}{2\sigma^2}} I_0\Big(\frac{\sqrt{b_0}A}{\sigma^2}\Big) &= \frac{1-\alpha}{2\sigma^2} e^{-\frac{b_0}{2\sigma^2}}, \\ e^{-\rho} I_0(\sqrt{2\rho}\beta) &= \frac{1-\alpha}{\alpha}. \end{aligned}$$

$I_0(x) \approx e^x/\sqrt{2\pi x}$ for larger values of x. Hence, at high SNR,

$$e^{-\rho} \frac{e^{(\sqrt{2\rho}\beta)}}{\sqrt{2\pi\sqrt{2\rho}\beta}} = \frac{1-\alpha}{\alpha}. \tag{2.12}$$

At high SNR, $\sqrt{b_0} \approx \frac{A}{2}$, since the distribution of square root of received signal samples becomes Gaussian [refer section 2.4.3] and consequently, $\beta \approx \sqrt{\frac{\rho}{2}}$. Hence, the approximate solution for β can be given as [3],

$$\beta = (1+\epsilon)\sqrt{\frac{\rho}{2}}, \tag{2.13}$$

where, ϵ is a correction factor. Substituting (2.13) in (2.12) yields $\epsilon = \frac{ln(2\pi\rho((1-\alpha)/\alpha)^2)}{2\rho}$. Figure 2.5 shows the BER plots with both the Gaussian threshold ($\beta \approx \sqrt{\frac{\rho}{2}}$) and the optimal threshold given in (2.13). It is clear that at high SNR, the optimal threshold approaches the Gaussian threshold value. At low SNR, the factor ϵ takes care of the deviation between both the thresholds. It is evident from (2.13) that the detection threshold is a function of SNR which has to be estimated. The SNR estimate is given by,

$$\hat{\rho} = \frac{\hat{A}^2}{2\hat{\sigma}^2} \tag{2.14}$$

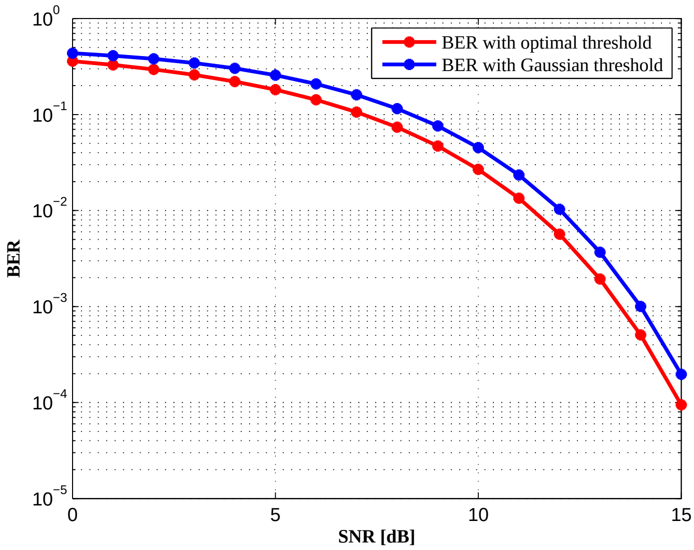

Figure 2.5: BER performance of non-coherent OOK receiver with Gaussian and optimal threshold.

where, $\hat{A}^2$ and $\hat{\sigma^2}$ are the signal and noise power estimates, respectively. The accuracy of the estimates is evaluated by normalized mean square error (NMSE) criterion. The NMSE of the SNR estimate is given by,

$$NMSE = \left(\frac{\rho - \hat{\rho}}{\rho}\right)^2. \tag{2.15}$$

In the following section, the NML detection technique is explained in detail.

2.3 Normalized max-zero likelihood (NML) detection

The detection performance of non coherent OOK receiver can be improved by the NML detection. The NML approach gives better results when we use matched filter after the square law detection. The technique is described in detail in 4 steps below.

Step 1 : Find the conditional likelihood $p(r_k|c_k = 0)$ of all the the received baseband samples (r_k) which is given by,

$$p(r_k|c_k = 0) = \frac{1}{2\sigma^2} e^{\frac{-r_k}{2\sigma^2}}, \qquad k = 1, 2, ..., N.$$

Step 2 : Find the maximum value of the likelihood, $p(r_k|c_k = 0)$.

$$p_{max} = max(p(r_k|c_k = 0)), \qquad k = 1, 2, ..., N. \tag{2.16}$$

Step 3 : Find the normalized max-zero likelihood given by,

$$p_n(r_k|c_k = 0) = \frac{p(r_k|c_k = 0)}{p_{max}}. \tag{2.17}$$

Step 4 : If $(p_n(r_k|c_k = 0) >= \kappa)$, decide $c_k = 0$, else decide $c_k = 1$. κ is the optimal soft decision threshold which is found through the Monte-Carlo simulation.

The NML detection technique is different from the maximum likelihood (ML) detection. In the ML detection, if $\frac{p(r_k|c_k=1)}{p(r_k|c_k=0)} > 1$, $c_k = 1$, else, $c_k = 0$.

Figures 2.6 and 2.7 show the curve fit plot of the threshold (κ) against SNR.

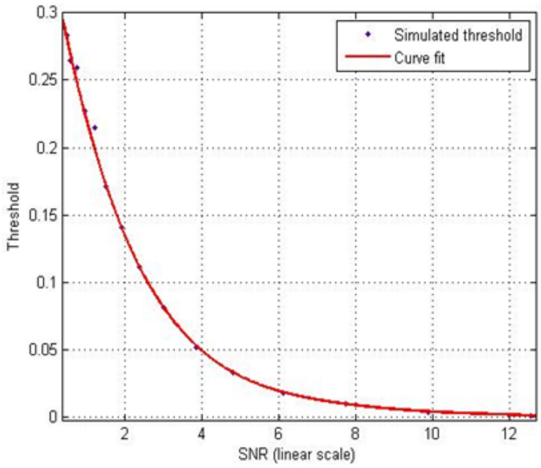

Figure 2.6: Curve fit plot of NML thresold (κ) against SNR for $SNR \leq 12$.

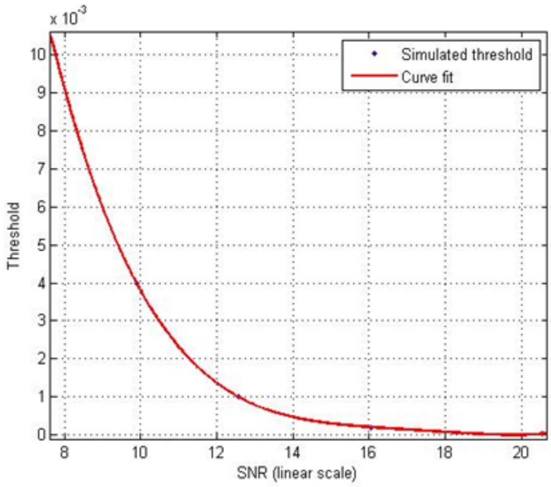

Figure 2.7: Curve fit plot of NML thresold (κ) against SNR for $SNR \geq 8 \leq 20$.

The curve fit equation is given below.

$$\kappa = \begin{cases} a_1\rho^5 + a_2\rho^4 + a_3\rho^3 + a_4\rho^2 + a_5\rho + a_6, & \text{if } \rho <= 12, \\ b_1\rho^4 + b_2\rho^3 + b_3\rho^2 + b_4\rho + b_5, & \text{if } \rho \geq 12 \leq 20. \end{cases}$$

For the case of $\rho > 20$, the threshold is approximated as,

$$\kappa = 2 \times 10^{-(10^{(\frac{\rho}{10})} - 8)}. \tag{2.18}$$

The coefficients are given in table 2.1.

Figures 2.8, 2.9 and 2.10 show the BER performance of the NML and ML detection techniques for symbol probability $\alpha = 0.3$, $\alpha = 0.5$ and $\alpha = 0.7$, respectively. It is evident that the NML method gives better detection performance when compared against the ML method. When the zeros are highly probable ($\alpha = 0.3$), gain of 1 dB is achieved at 2×10^{-4} BER by the NML method. It is also to be noted that the gain decreases when α increases. Under equiprobable symbol condition ($\alpha = 0.5$), the gain reduces to 0.6 dB and it reduces further to 0.3 dB for $\alpha = 0.7$. The reason for the reduction in gain with increase in α is straight forward as the NML detection is based on the zeros. Higher the probability of zero, better the detection performance.

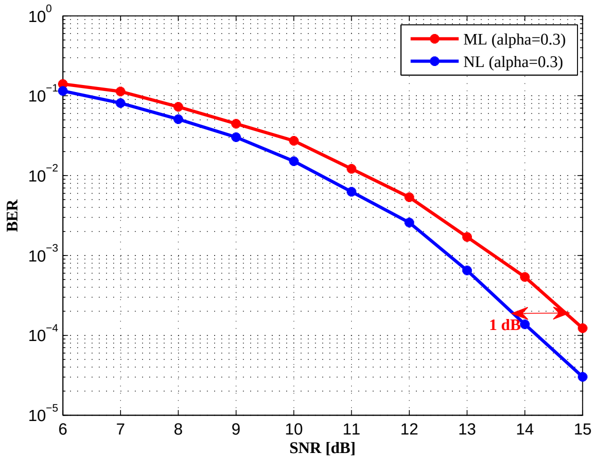

Figure 2.8: BER versus SNR is shown for NML and ML non-coherent detection of OOK signals for $\alpha = 0.3$.

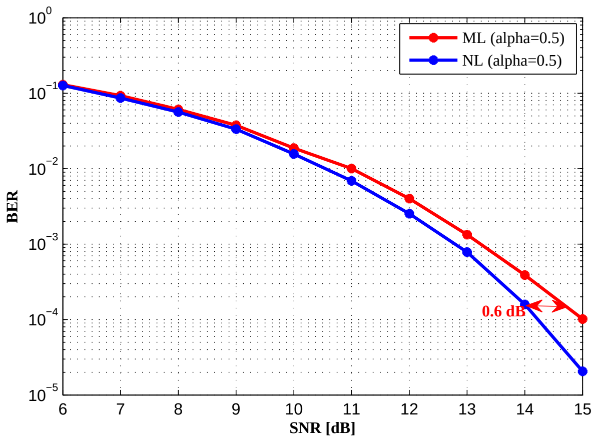

Figure 2.9: BER versus SNR is shown for NML and ML non-coherent detection of OOK signals for $\alpha = 0.5$.

In the following section, DA SNR estimators are explained in detail and their NMSE performance is analyzed.

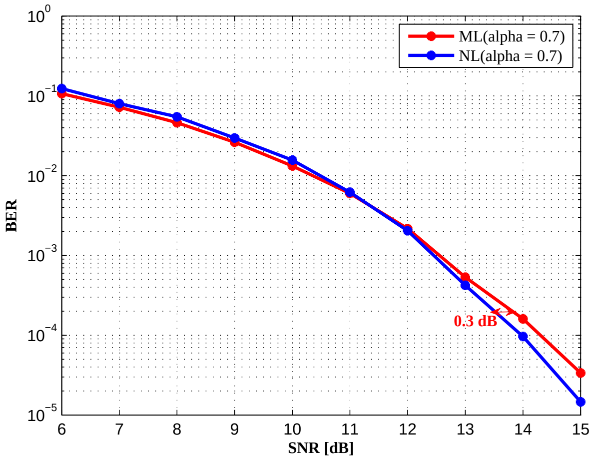

Figure 2.10: BER versus SNR is shown for NML and ML non-coherent detection of OOK signals for $\alpha = 0.7$.

Table 2.1: Coefficients: NML detection

Cofficients	Value	Cofficients	Value
a_1	-3.597e-6	b_1	1.347e-06
a_2	0.0001702	b_2	-9.049e-05
a_3	-0.003244	b_3	0.00228
a_4	0.03152	b_4	-0.02564
a_5	-0.1598	b_5	0.1091
a_6	0.3516	–	–

2.4 DA estimation

The DA estimation is carried out in the case of known preamble structure. The DA estimators considered here are the ML and M_1V estimators.

2.4.1 ML estimator

Consider the case of known symbol sequence, $C_K = [1 \dots 1]^T$. The pdf of r_k is the non central Chi-square distribution function. The joint pdf of R_K is obtained as,

$$p(R_K) = \prod_{j=0}^{K-1} \frac{1}{2\sigma^2} e^{-\frac{r_j + A^2}{2\sigma^2}} I_0\Big(\frac{\sqrt{r_j}A}{\sigma^2}\Big). \tag{2.19}$$

The log likelihood function of (2.19) is given as,

$$\Lambda(R_K; A; \sigma^2) = -Kln(2\sigma^2) - \frac{1}{2\sigma^2}\left[\sum_{j=0}^{K-1} r_j + KA^2\right] + \sum_{j=0}^{K-1} ln[I_0\Big(\frac{\sqrt{r_j}A}{\sigma^2}\Big)]. \tag{2.20}$$

To obtain an estimate for the amplitude of the signal, (2.20) is partially differentiated with respect to A and equated to '$0'$ as shown below.

$$\frac{\partial \Lambda(R_K; A; \sigma^2)}{\partial A} = \frac{-KA}{\sigma^2} + \sum_{j=0}^{K-1} \frac{I_1\left(\frac{\sqrt{r_j}A}{\sigma^2}\right)}{I_0\left(\frac{\sqrt{r_j}A}{\sigma^2}\right)} \frac{\sqrt{r_j}}{\sigma^2}. \tag{2.21}$$

Considering $I_1(x)/I_0(x) \approx 1$ for larger values of x, i.e., at high SNR and equating (2.21) to 0 gives,

$$\sum_{j=0}^{K-1} \sqrt{r_j} = AK,$$

The ML amplitude estimate $\hat{A}_{ML}$, is given as,

$$\hat{A}_{ML} = \frac{1}{K} \sum_{j=0}^{K-1} \sqrt{r_j}. \tag{2.22}$$

Similarly, to obtain an estimate for the noise variance, (2.20) is partially differentiated with respect to σ^2 and equated to '$0'$.

$$\frac{\partial \Lambda(R_K; A; \sigma^2)}{\partial \sigma^2} = -\frac{K}{\sigma^2} + \frac{1}{2(\sigma^2)^2}\left[\sum_{j=0}^{K-1} r_j + KA^2\right] - \frac{A}{(\sigma^2)^2} \sum_{j=0}^{K-1} \frac{I_1\left(\frac{\sqrt{r_j}A}{\sigma^2}\right)}{I_0\left(\frac{\sqrt{r_j}A}{\sigma^2}\right)} \sqrt{r_j}. \tag{2.23}$$

Simplifying with the assumption of high SNR and equating to 0, the noise variance estimate $(2\hat{\sigma}^2_{ML})$ is obtained as,

$$2\hat{\sigma}^2_{ML} = \frac{1}{K}\left[\sum_{j=0}^{K-1} r_j - K\hat{A}^2_{ML}\right]. \tag{2.24}$$

The SNR estimate is obtained from $\hat{A}_{ML}$ and $\hat{\sigma}^2_{ML}$ using (2.14).

2.4.2 M_1V estimator

M_1V estimator is based on the first moment (M_1) and the first central moment (V) of R_K, respectively. Consider the known sequence $C_K = [1 \ldots 1]^T$. The approximate l^{th} moment and the first central moment of the elements of R_K can be computed as, [13],

$$\begin{aligned} \hat{M}_l &= \frac{1}{K} \sum_{j=0}^{K-1} r_j^l, \\ \hat{V} &= \hat{M}_2 - \hat{M}_1^{\,2}. \end{aligned} \tag{2.25}$$

M_1 and V for the non central Chi-square distributed random variable r_k is given as, [4],

$$\begin{aligned} M_1 &= 2\sigma^2 + A^2, \\ V &= 4\sigma^4 + 4\sigma^2 A^2. \end{aligned}$$

The estimates are obtained by solving the above equations for $\sigma^2_{M_1V}$ and $\hat{A}^2_{M_1V}$ and are given as,

$$
\begin{aligned}
2\hat{\sigma}^2_{M_1V} &= \hat{M}_1 - \sqrt{\hat{M}_1^{\ 2} - V}, && (2.26)\\
\hat{A}^2_{M_1V} &= \hat{M}_1 - 2\hat{\sigma}^2_{M_1V}. && (2.27)
\end{aligned}
$$

The M_1V SNR estimate is obtained from $\hat{A}_{M_1V}$ and $\hat{\sigma}^2_{M_1V}$ using (2.14).

2.4.3 Cramer-Rao lower bound (CRLB) for DA SNR estimation

The joint pdf of the square root of received baseband signal samples is given by [3],

$$p(Z) = \prod_{j=0}^{K-1} \frac{z_j}{\sigma^2} e^{-\frac{z_j^2+A^2}{2\sigma^2}} I_0\Big(\frac{z_j A}{\sigma^2}\Big), \tag{2.28}$$

where $Z = [z_0 \ldots z_{K-1}]^T$ and $z_j = \sqrt{r_j}$. $I_0(x) \approx e^x/\sqrt{2\pi x}$ for larger values of x and $\frac{z_j}{A} \approx 1$ at high SNR. This leads to the simplification of (2.28) as,

$$
\begin{aligned}
p(Z) &= \prod_{j=0}^{K-1} \frac{z_j}{\sigma^2\sqrt{2\pi z_j A/\sigma^2}} e^{-\frac{z_j^2+A^2}{2\sigma^2}} e^{z_j A/\sigma^2},\\
p(Z) &= \prod_{j=0}^{K-1} \frac{1}{\sqrt{2\pi\sigma^2}} e^{-\frac{(z_j-A)^2}{2\sigma^2}}. && (2.29)
\end{aligned}
$$

The log likelihood function of (2.29) is given by,

$$\Lambda_{CRLB}(Z; A; \sigma^2) = -\frac{K}{2} ln(2\pi\sigma^2) - \frac{1}{2\sigma^2} \sum_{j=0}^{K-1} (z_j - A)^2 \tag{2.30}$$

Let θ=[A σ^2]. The transformation function, $\mathbf{g}(\theta) = \frac{A^2}{2\sigma^2}$. $CRLB_{DA}$ is given by [18],

$$CRLB_{DA} = \frac{\partial \mathbf{g}(\theta)}{\partial\theta} \mathcal{I}^{-1} \frac{\partial \mathbf{g}(\theta)^T}{\partial\theta}, \tag{2.31}$$

where, $\mathcal{I}$ is the Fisher information matrix for $\Lambda_{CRLB}(Z; A; \sigma^2)$ which is given by,

$$\mathcal{I} = \begin{bmatrix} -E\Big[\frac{\partial^2 \Lambda_{CRLB}(Z;A;\sigma^2)}{\partial A^2}\Big] & -E\Big[\frac{\partial^2 \Lambda_{CRLB}(Z;A;\sigma^2)}{\partial A \partial\sigma^2}\Big] \\ -E\Big[\frac{\partial^2 \Lambda_{CRLB}(Z;A;\sigma^2)}{\partial\sigma^2 \partial A}\Big] & -E\Big[\frac{\partial^2 \Lambda_{CRLB}(Z;A;\sigma^2)}{\partial{\sigma^2}^2}\Big] \end{bmatrix}. \tag{2.32}$$

where,

$$\begin{aligned}
-E\Big[\frac{\partial^2\Lambda_{CRLB}(Z;A;\sigma^2)}{\partial A^2}\Big] &= \frac{K}{\sigma^2},\\
-E\Big[\frac{\partial^2\Lambda_{CRLB}(Z;A;\sigma^2)}{\partial A\partial\sigma^2}\Big] &= 0,\\
-E\Big[\frac{\partial^2\Lambda_{CRLB}(Z;A;\sigma^2)}{\partial\sigma^2\partial A}\Big] &= 0,\\
-E\Big[\frac{\partial^2\Lambda_{CRLB}(Z;A;\sigma^2)}{\partial{\sigma^2}^2}\Big] &= \frac{K}{2\sigma^4}.
\end{aligned} \tag{2.33}$$

$\mathcal{I}$ is given by,

$$\mathcal{I} = \begin{bmatrix} \frac{K}{\sigma^2} & 0 \\ 0 & \frac{K}{2\sigma^4} \end{bmatrix}. \tag{2.34}$$

$\frac{\partial \mathbf{g}(\theta)}{\partial\theta}$ is given by,

$$\frac{\partial \mathbf{g}(\theta)}{\partial\theta} = \begin{bmatrix} \frac{A}{\sigma^2} & -\frac{A^2}{2\sigma^4} \end{bmatrix}. \tag{2.35}$$

Substituting $\rho = \frac{A^2}{2\sigma^2}$ and combining (2.34), (2.31) and (2.35) gives the expression for $CRLB_{DA}$ and normalized CRLB ($NCRLB_{DA}$) as,

$$\begin{aligned}
CRLB_{DA} &= \frac{2}{K}[\rho+\rho^2],\\
NCRLB_{DA} &= \frac{CRLB_{DA}}{\rho^2} = \frac{2}{K}\Bigg[1+\frac{1}{\rho}\Bigg].
\end{aligned} \tag{2.36}$$

(2.36) is similar to the $NCRLB_{NDA}$ of $MQAM$ constellations given in [15] as the simplification using high SNR assumption has led to similar pdfs for both cases. In the following section, the NMSE performance of the DA estimators is discussed in detail.

2.4.4 NMSE performance of DA estimators

The NMSE of the SNR estimators is given by (2.15). Figure 2.11 shows the NMSE performance of the ML and M_1V DA estimators. The preamble length (K) is assumed to be 32 bits and the NMSE performance is determined by 500 Monte-Carlo simulation runs. The asymptotic NCRLB is also shown which gives the lower bound on the NMSE performance. It can be seen that the M_1V estimator performs better than the ML estimator at low SNR region. This is because of the high SNR approximation of the Bessel function in the case of ML estimator. At high SNR, the performance of ML estimator is equivalent to that of M_1V estimator.

Figure 2.12 shows the plot of mean of the SNR estimates of both the estimators against the true SNR. As it can be seen, the M_1V and ML SNR estimates become close to each other for SNR> 5 dB.

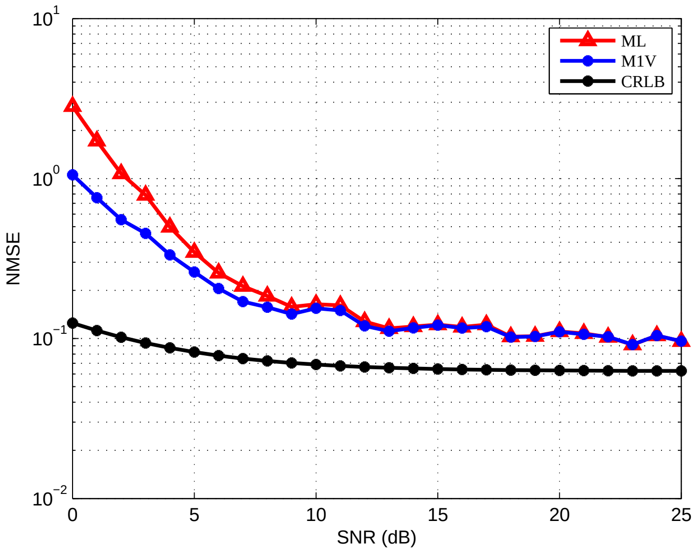

Figure 2.11: NMSE performance is compared against SNR for ML and M_1V DA estimators for $K = 32$ bits and the normalized CRLB is plotted against SNR for DA estimation.

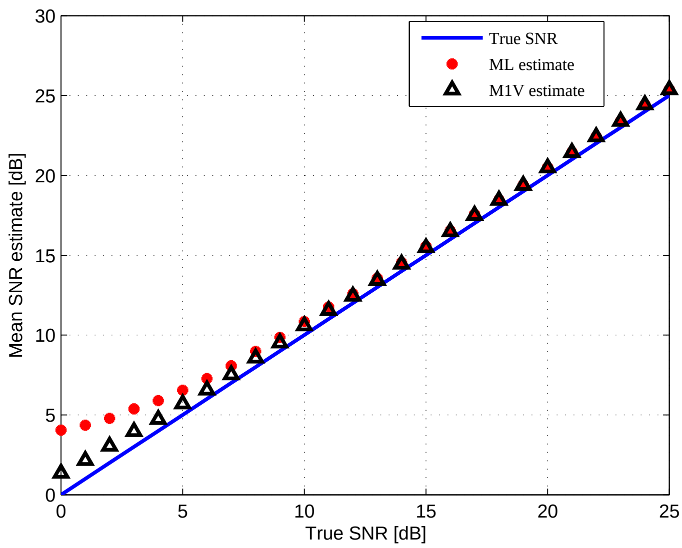

Figure 2.12: Mean SNR estimate [dB] versus true SNR [dB] for ML and M_1V DA estimators for $K = 32$ bits.

2.5 NDA estimation

NDA estimation is carried out in the case of unknown data sequence. Let $C_N = [c_0 \dots c_{N-1}]^T$ be the unknown data sequence. The unconditional pdf of r_k can be expressed as,

$$p(r_k) \;=\; \frac{\alpha}{2\sigma^2} e^{-\frac{r_k + A^2}{2\sigma^2}} I_0\left(\frac{\sqrt{r_k}A}{\sigma^2}\right) + \frac{1-\alpha}{2\sigma^2} e^{-\frac{r_k}{2\sigma^2}}. \tag{2.37}$$

It is difficult to obtain a closed form ML solution for the pdf described in (2.37). Therefore, M_1M_2, M_2M_3 and EM estimators are proposed for NDA estimation to come close to the ML solution. In the following section moments based NDA SNR estimators are explained in detail.

2.5.1 Moments based NDA SNR estimators

The l^{th} order true moment of a random variable q with a pdf $f(q)$ is given as,

$$\begin{aligned} M_l &= E[r^l], \\ &= \int_{-\infty}^{\infty} q^l f(q) \quad dq \end{aligned} \tag{2.38}$$

M_1, M_2 and M_3 of r_k are obtained using (2.38) and (2.37) as given below.

$$\begin{aligned} M_1 &= \int_0^{\infty} r_k p(r_k) \quad dr_k, \\ &= \alpha \int_0^{\infty} \frac{r_k}{2\sigma^2} e^{-\frac{r_k+A^2}{2\sigma^2}} I_0\Big(\frac{\sqrt{r_k}A}{\sigma^2}\Big) \quad dr_k + (1-\alpha)\int_0^{\infty} \frac{r_k}{2\sigma^2} e^{-\frac{r_k}{2\sigma^2}} \quad dr_k, \\ &= \alpha(2\sigma^2 + A^2) + (1-\alpha)2\sigma^2, \\ &= 2\sigma^2 + A^2\alpha. \end{aligned} \tag{2.39}$$

$$\begin{aligned} M_2 &= \int_0^{\infty} r_k^2 p(r_k) \quad dr_k, \\ &= \alpha \int_0^{\infty} \frac{r_k^2}{2\sigma^2} e^{-\frac{r_k+A^2}{2\sigma^2}} I_0\Big(\frac{\sqrt{r_k}A}{\sigma^2}\Big) \quad dr_k + (1-\alpha)\int_0^{\infty} \frac{r_k^2}{2\sigma^2} e^{-\frac{r_k}{2\sigma^2}} \quad dr_k, \\ &= \alpha(8\sigma^4 + 8\sigma^2A^2 + A^4) + (1-\alpha)8\sigma^4, \\ &= 8\sigma^4 + 8\alpha\sigma^2A^2 + A^4. \end{aligned} \tag{2.40}$$

$$\begin{aligned} M_3 &= \int_0^{\infty} r_k^3 p(r_k) \quad dr_k, \\ &= \alpha \int_0^{\infty} \frac{r_k^3}{2\sigma^2} e^{-\frac{r_k+A^2}{2\sigma^2}} I_0\Big(\frac{\sqrt{r_k}A}{\sigma^2}\Big) \quad dr_k + (1-\alpha)\int_0^{\infty} \frac{r_k^3}{2\sigma^2} e^{-\frac{r_k}{2\sigma^2}} \quad dr_k, \\ &= \alpha(48\sigma^6 + 72A^2\sigma^4 + 18A^4\sigma^2 + A^6) + (1-\alpha)48\sigma^6, \\ &= 48\sigma^6 + 72\alpha A^2\sigma^4 + 18\alpha A^4\sigma^2 + \alpha A^6. \end{aligned} \tag{2.41}$$

In the following section, M_1M_2 estimator is explained in detail

2.5.1.1 M_1M_2 Estimator

M_1M_2 estimator is based on the first and second moments of the elements of R_N. $\hat{M}_1$ and $\hat{M}_2$ are computed as mentioned in (2.25). M_1 and M_2 for r_k are given in (2.39) and (2.40), respectively. The estimates $\hat{A}^2_{M_1M_2}$ and $\hat{\sigma}^2_{M_1M_2}$ can be obtained by solving (2.39) and (2.40) as,

$$\hat{\sigma}^2_{M_1M_2} = \frac{\hat{M}_1}{2} + \frac{\sqrt{2\alpha\hat{M}_1^2(2\alpha-1) - 2\hat{M}_2\alpha^2 + \alpha\hat{M}_2}}{4\alpha-2}, \quad (2.42)$$

$$\hat{A}^2_{M_1M_2} = \frac{\hat{M}_1 - 2\hat{\sigma}^2_{M_1M_2}}{\alpha}. \quad (2.43)$$

Using (2.43), (2.42) and (2.14), SNR estimate can be evaluated.
Let us consider the case of $\alpha = 1/2$. The moments are given by,

$$\begin{aligned} M_1 &= 2\sigma^2 + \frac{A^2}{2}, \\ M_2 &= 8\sigma^4 + 4\sigma^2A^2 + \frac{A^4}{2}, \\ &= 2M_1^2. \end{aligned}$$

Since, $M_2 = 2M_1^2$ for $\alpha = 1/2$, M_1M_2 estimator does not yield the solution for SNR estimate when the symbols are equiprobable. Therefore, it is necessary to look at higher order moments to account for the equiprobable symbol condition. The following section describes the higher order M_2M_3 estimator.

2.5.1.2 M_2M_3 Estimator

M_2M_3 estimator is based on the second and third moments of the elements of R_N. This estimator has been developed for the equiprobable case ($\alpha = 1/2$). $\hat{M}_2$ and $\hat{M}_3$ are computed as mentioned in (2.25). M_2 and M_3 for r_k are given by (2.40) and (2.41), respectively. Considering equiprobable symbol condition ($\alpha = 1/2$), (2.40) and (2.41) can be rewritten as,

$$\begin{aligned} M_2 &= 8\sigma^4 + 4\sigma^2A^2 + \frac{A^4}{2}, \\ M_3 &= \frac{1}{2}(96\sigma^6 + 72A^2\sigma^4 + 18A^4\sigma^2 + A^6). \end{aligned}$$

The above equations are solved to yield the expressions for the estimates $\hat{A}^2_{M_2M_3}$ and $\hat{\sigma}^2_{M_2M_3}$ as given below.

$$\hat{A}^2_{M_2M_3} = \sqrt[3]{6\sqrt{2}\hat{M}_2^{3/2} - 4\hat{M}_3}, \quad (2.44)$$

$$\hat{\sigma}^2_{M_2M_3} = \frac{\sqrt{2\hat{M}_2} - \hat{A}^2_{M_2M_3}}{4}. \quad (2.45)$$

Using (2.14), (2.44) and (2.45), the SNR estimate can be evaluated. The performance of M_1M_2 and M_2M_3 estimators degrade at high SNR. The degradation is due to the increased error in noise power estimates at high SNR. The approximate expressions for the error in the A^2 estimates (ΔA^2) and σ^2 estimates ($\Delta\sigma^2$) can be expressed in terms of the error in the moments estimates. Let ΔM_2 and ΔM_3 be the error in estimates of M_2 and M_3 respectively. Now, (2.44) can be rewritten as,

$$\begin{aligned}
\hat{A}^2_{M_2M_3} &= \Big(6\sqrt{2}(M_2+\Delta M_2)^{3/2} - 4(M_3+\Delta M_3)\Big)^{1/3}, \\
&= \Big(6\sqrt{2}M_2^{3/2}\Big(1+\frac{M_2}{\Delta M_2}\Big)^{3/2} - 4M_3 - 4\Delta M_3\Big)^{1/3}, \\
&\approx \Big(6\sqrt{2}M_2^{3/2}\Big(1+\frac{3M_2}{2\Delta M_2}\Big) - -4M_3 - 4\Delta M_3\Big)^{1/3}, \\
&\approx \Big(6\sqrt{2}{M_2}^{3/2} - 4M_3 + \frac{18\sqrt{2}M_2^{3/2}\Delta M_2}{2M_2} - 4\Delta M_3\Big)^{1/3}, \\
&\approx (6\sqrt{2}{M_2}^{3/2} - 4M_3)^{1/3}\Big(1+\frac{9\sqrt{2M_2}\Delta M_2 - 4\Delta M_3}{6\sqrt{2}{M_2}^{3/2} - 4M_3}\Big)^{1/3}, \\
\hat{A}^2_{M_2M_3} &\approx (6\sqrt{2}{M_2}^{3/2} - 4M_3)^{1/3} + \frac{9\sqrt{2M_2}\Delta M_2 - 4\Delta M_3}{3(6\sqrt{2}{M_2}^{3/2} - 4M_3)^{2/3}}. \qquad (2.46)
\end{aligned}$$

Similarly (2.45) can be rewritten as,

$$\begin{aligned}
\hat{\sigma}^2_{M_2M_3} &= \frac{\sqrt{2(M_2+\Delta M_2)} - (A^2_{M_2M_3} + \Delta A^2)}{4}, \\
&= \frac{\sqrt{2M_2\Big(1+\frac{\Delta M_2}{M_2}\Big)} - A^2 - \Delta A^2}{4}, \\
&\approx \frac{\sqrt{2M_2} - A^2}{4} + \frac{\frac{\Delta M_2}{\sqrt{2M_2}} - \Delta A^2}{4}, \\
\hat{\sigma}^2_{M_2M_3} &\approx \frac{\sqrt{2M_2} - A^2}{4} + \Delta\sigma^2, \qquad (2.47)
\end{aligned}$$

where,

$$\begin{aligned}
\Delta A^2 &= \frac{9\sqrt{2M_2}\Delta M_2 - 4\Delta M_3}{3(6\sqrt{2}{M_2}^{3/2} - 4M_3)^{2/3}}, \\
\Delta\sigma^2 &= \frac{\frac{\Delta M_2}{\sqrt{2M_2}} - \Delta A^2}{4}.
\end{aligned}$$

The effects of the error in the moments are reflected in the poor noise estimates at high

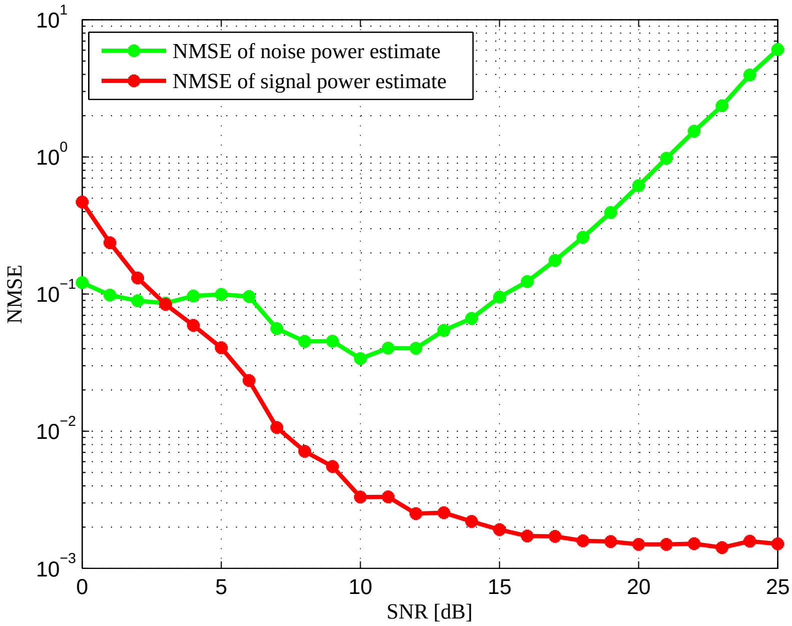

Figure 2.13: NMSE versus SNR [dB] for estimates of A^2 and $2\sigma^2$ for $N = 512$ bits and $\alpha = 1/2$.

SNR. This is shown in figure 2.13. It is evident from figure 2.13 that the amplitude estimates are better at high SNR, whereas, the noise estimates degrade at high SNR. This results in unreliable SNR estimates at high SNR. EM estimator is proposed to overcome the problem in the high SNR region.

2.5.2 EM estimator

EM estimation is an iterative procedure, [19]. The convergence tolerance shall be set to a constant value, $\tau \ll 1$ and let m be the maximum number of iterations. The joint pdf of the elements of R_N conditioned on the elements of C_N is given as,

$$p(R_N|C_N) = \prod_{k=0}^{N-1} \frac{1}{2\sigma^2} e^{-\frac{r_k + A^2 c_k^2}{2\sigma^2}} I_0\Big(\frac{\sqrt{r_k} A c_k}{\sigma^2}\Big).$$

The log likelihood of $p(R_N|C_N)$ is given as,

$$\begin{aligned}\Lambda_{EM}(R_N; A; \sigma^2) &= -N ln(2\sigma^2) - \frac{1}{2\sigma^2}\Bigg[\sum_{k=0}^{N-1} r_k + A^2 \sum_{k=0}^{N-1} c_k^2\Bigg] \\ &\quad + \sum_{k=0}^{N-1} ln\Bigg(I_0\Big(\frac{\sqrt{r_k} A c_k}{\sigma^2}\Big)\Bigg).\end{aligned}$$

The EM algorithm involves four steps.

Step 1: Calculation of expectation
Find the expectation of $\Lambda_{EM}(R_N; A; \sigma^2)$ with respect to c_k as,

$$\begin{aligned}\Psi(R_N; A; \sigma^2) &= E_{c_k}[\Lambda_{EM}(R_N; A; \sigma^2)].\\ &= -Nln(2\sigma^2) - \frac{1}{2\sigma^2}\Bigg[\sum_{k=0}^{N-1} r_k + A^2 \sum_{k=0}^{N-1} E_{c_k}[c_k^2]\Bigg]\\ &\quad + \sum_{k=0}^{N-1} E_{c_k}\Bigg[ln\Bigg(I_0\Big(\frac{\sqrt{r_k}Ac_k}{\sigma^2}\Big)\Bigg)\Bigg]. \end{aligned} \tag{2.48}$$

At the start of n^{th} iteration,

$$\begin{aligned} E_{c_k}[c_k^2] &= \sum_{i=0}^{1} P_{ik,n-1} i^2\\ &= P_{1k,n-1}, \end{aligned} \tag{2.49}$$

$$\begin{aligned} E_{c_k}\Bigg[ln\Bigg(I_0\Big(\frac{\sqrt{r_k}Ac_k}{\sigma^2}\Big)\Bigg)\Bigg] &= \sum_{i=0}^{1} P_{ik,n-1} ln\Bigg(I_0\Big(\frac{\sqrt{r_k}Ai}{\sigma^2}\Big)\Bigg)\\ &= P_{1k,n-1} ln\Bigg(I_0\Big(\frac{\sqrt{r_k}A}{\sigma^2}\Big)\Bigg), \end{aligned} \tag{2.50}$$

where, $P_{ik,n-1}$ is the probability of '$c_k = i$' at the $(n-1)^{th}$ iteration given by,

$$\begin{aligned} P_{ik,n-1} &= P(c_k = i | r_k; A_{n-1}, \sigma_{n-1})\\ &= \frac{P(r_k | c_k = i; A_{n-1}, \sigma_{n-1}) P(c_k = i)}{P(r_k; A_{n-1}, \sigma_{n-1})}, \end{aligned}$$

where,

$$\begin{aligned} P(c_k = i) &= \begin{cases} \alpha, & \text{if } i = 1,\\ 1-\alpha, & \text{if } i = 0, \end{cases}\\ P(r_k | c_k = i; A_{n-1}, \sigma_{n-1}) &= \frac{1}{2\sigma_{n-1}^2} e^{-\frac{r_k + A_{n-1}^2 i^2}{2\sigma_{n-1}^2}} I_0\Big(\frac{\sqrt{r_k}A_{n-1}i}{\sigma_{n-1}^2}\Big),\\ P(r_k; A_{n-1}, \sigma_{n-1}) &= \sum_{i=0}^{1} P(r_k | c_k = i; A_{n-1}, \sigma_{n-1}) P_i. \end{aligned}$$

Combining (2.48), (2.49) and (2.50),

$$\begin{aligned}\Psi(R_N; A; \sigma^2) &= -Nln(2\sigma^2) - \frac{1}{2\sigma^2}\Bigg[\sum_{k=0}^{N-1} r_k + A^2 \sum_{k=0}^{N-1} P_{1k,n-1}\Bigg]\\ &\quad + \sum_{k=0}^{N-1} P_{1k,n-1} ln\Bigg(I_0\Big(\frac{\sqrt{r_k}A}{\sigma^2}\Big)\Bigg). \end{aligned} \tag{2.51}$$

Step 2: Maximization of expectation
Maximize $\Psi(R_N; A; \sigma^2)$ with respect to the arguments A and σ^2. Let θ_n=$[A_n \ \sigma_n^2]$ be the value of the arguments at the end of n^{th} iteration. θ_n is given by,

$$\theta_n = \arg\max_{A;\sigma^2}[\Psi(R_N; A; \sigma^2)].$$

The values for A_n and σ_n^2 at the end of n^{th} iteration are obtained by partially differentiating (2.51) with respect to A and σ^2 and equating to 0 as given below.

$$\frac{\partial \Psi(R_N; A; \sigma^2)}{\partial A} = \frac{-A\sum_{k=0}^{N-1} P_{1k,n-1}}{\sigma^2} + \sum_{k=0}^{N-1} P_{1k,n-1} \frac{I_1\left(\frac{\sqrt{r_k}A}{\sigma^2}\right)}{I_0\left(\frac{\sqrt{r_k}A}{\sigma^2}\right)} \frac{\sqrt{r_k}}{\sigma^2}. \tag{2.52}$$

$$\begin{aligned}\frac{\partial \Psi(R_N; A; \sigma^2)}{\partial \sigma^2} &= -\frac{N}{\sigma^2} + \frac{1}{2(\sigma^2)^2}\left[\sum_{k=0}^{N-1} r_k + A^2 \sum_{k=0}^{N-1} P_{1k,n-1}\right], \\ &\quad - \frac{A}{(\sigma^2)^2}\sum_{k=0}^{N-1} P_{1k,n-1} \frac{I_1\left(\frac{\sqrt{r_k}A}{\sigma^2}\right)}{I_0\left(\frac{\sqrt{r_k}A}{\sigma^2}\right)} \sqrt{r_k}..\end{aligned} \tag{2.53}$$

After high SNR approximation, equating (2.52) and (2.53) to '0' gives,

$$A_n = \frac{\sum_{k=0}^{N-1} P_{1k,n-1}\sqrt{r_k}}{\sum_{k=0}^{N-1} P_{1k,n-1}}. \tag{2.54}$$

$$2\sigma_n^2 = \frac{1}{N}\left[\sum_{k=0}^{N-1} r_k - A_n^2 \sum_{k=0}^{N-1} P_{1k,n-1}\right]. \tag{2.55}$$

Step 3: Compute the SNR estimate $\rho_n = \frac{A_n^2}{2\sigma_n^2}$ at the end of n^{th} iteration. If τ or m is reached, recalibrate the noise estimation. Otherwise, continue with the iteration procedure.

Step 4: Recalibration of the noise estimation
It is found that the noise estimation after convergence of the EM algorithm is biased. This is due to the fact that the noise estimate at the end of each iteration is based on the signal samples which constitute both amplitude and noise. Recalibration is an additional step employed to remove any significant bias in the noise estimation. After convergence, noise is re-estimated from the knowledge of the vector $\mathcal{P}_{0,n} = [P_{00,n}P_{02,n}\ldots P_{0N-1,n}]^T$. The structure of the elements of $\mathcal{P}_{0,n}$ is given below.

$$P_{0k,n} \approx \begin{cases} 1, & \text{if } c_k = 0, \\ 0, & \text{if } c_k = 1. \end{cases}$$

Due to the above structure, the noise power $2\sigma_n^2$ shall be recalibrated as shown below.

$$2\sigma_n^2 = \frac{\sum_{k=0}^{N-1} P_{0k,n} r_k}{\sum_{k=0}^{N-1} P_{0k,n}}. \tag{2.56}$$

Using (2.14), (2.54) and (2.56), the SNR estimate can be evaluated.

2.5.3 Hybrid estimators

The high SNR approximation results in a significant bias in the estimates of EM estimator in the low SNR region. The moments based estimators perform better at this region. Hence, hybrid $M_1M_2 - EM$ and $M_2M_3 - EM$ estimators are proposed to overcome the limitations. The SNR is estimated by the moments based estimators up to a certain threshold point, ρ_0. EM estimator is used to estimate SNR greater than ρ_0. The performance of hybrid estimators is described in detail in section 2.5.4.

In the following section, the NMSE performance of the NDA estimators is discussed in detail.

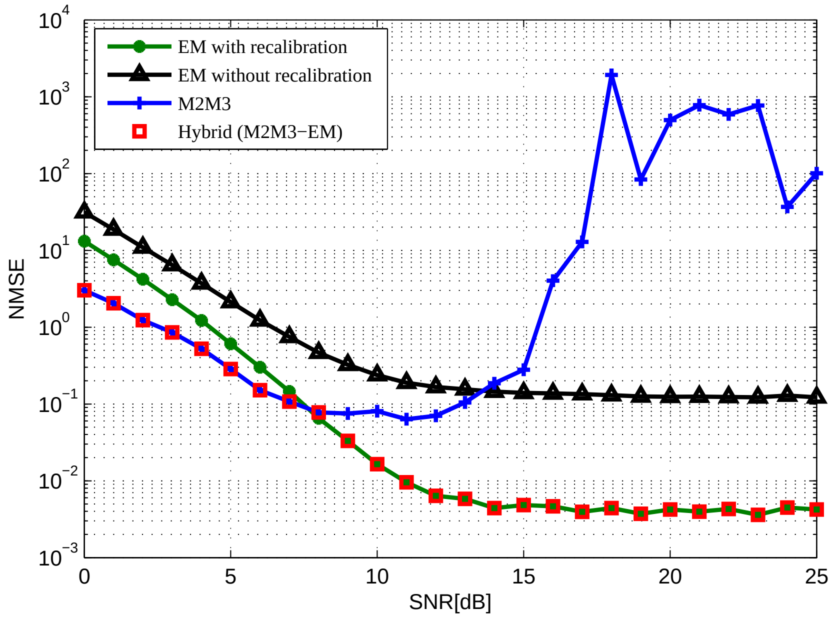

Figure 2.14: NMSE versus SNR [dB] for EM, M_2M_3 and $M_2M_3 - EM$ NDA estimators for $N = 512$ bits and $\alpha = 1/2$.

2.5.4 NMSE performance of NDA estimators

The NMSE performance of the NDA estimators is evaluated through simulation. The estimators are simulated for packet length, $N = 512$ bits. Equiprobable symbol condition is assumed during simulation of M_2M_3 and $M_2M_3 - EM$ estimators. M_1M_2 and $M_1M_2 - EM$ estimators are simulated for the condition of $\alpha = 1/3$. The EM

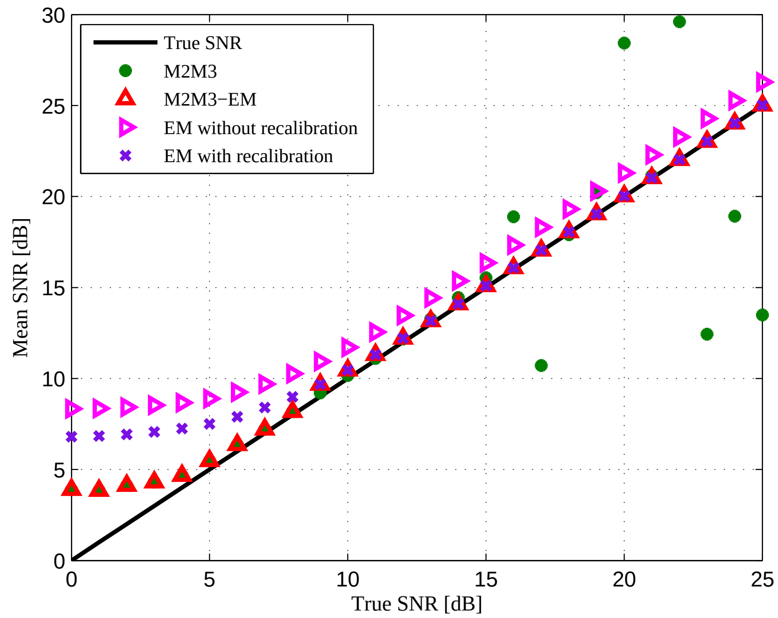

Figure 2.15: Mean SNR estimate [dB] versus true SNR [dB] for M_2M_3, EM and $M_2M_3 - EM$ NDA estimators for $N = 512$ bits and $\alpha = 1/2$.

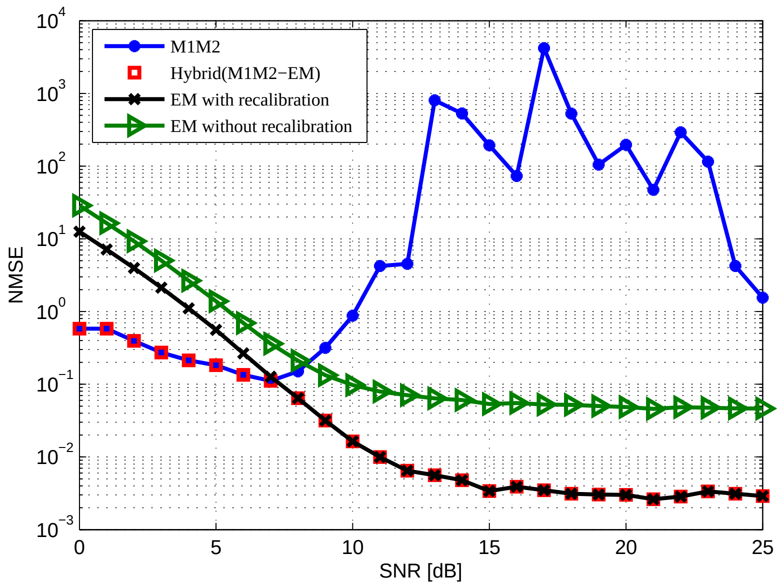

Figure 2.16: NMSE versus SNR [dB] for EM, M_1M_2 and $M_1M_2 - EM$ NDA estimators for $N = 512$ bits and $\alpha = 1/3$.

algorithm is initialized with θ_0=[100 1]. The convergence tolerence, τ is set to 10^-6 and the maximum number of iterations, m is set to 5.

Figure 2.14 shows the NMSE performance of the M_2M_3, EM and $M_2M_3 - EM$ estimators. The performance of M_2M_3 estimator degrades for SNR> 8 dB. This is due

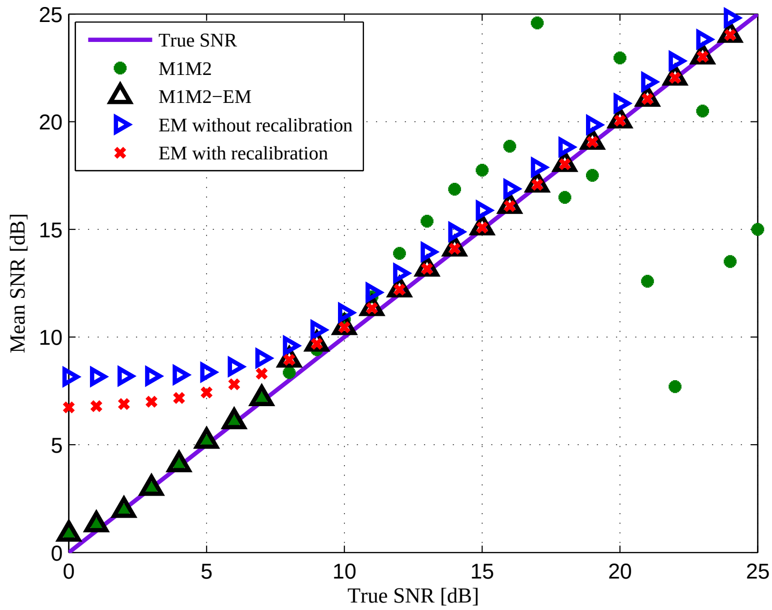

Figure 2.17: Mean SNR estimate [dB] versus true SNR [dB] for M_1M_2, EM and $M_1M_2 - EM$ NDA estimators for $N = 512$ bits and $\alpha = 1/3$.

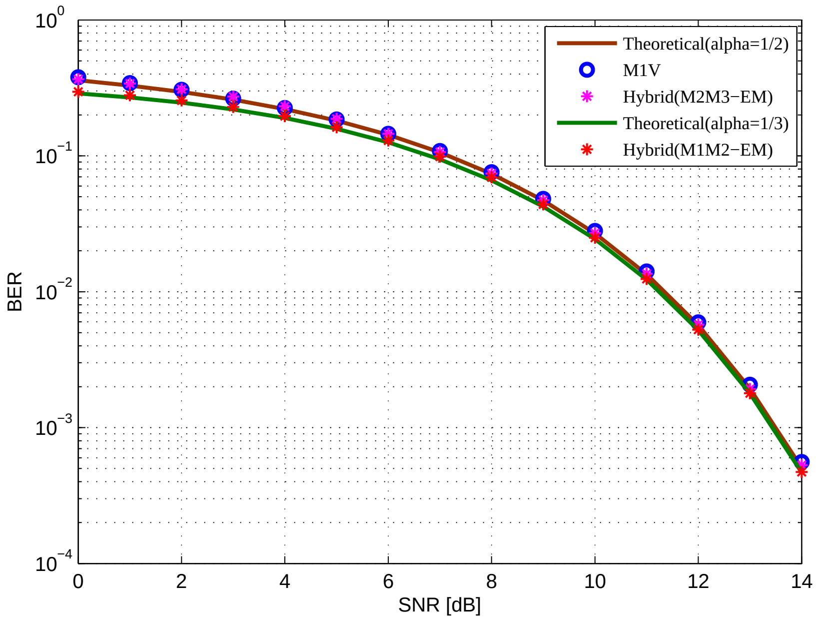

Figure 2.18: BER versus SNR [dB] is shown for M_1V DA estimator and $M_2M_3 - EM$ NDA estimator for $\alpha = 1/2$ and $M_1M_2 - EM$ NDA estimator for $\alpha = 1/3$. $N = 512$ bits for all the cases. Theoretical BER versus SNR [dB] for $\alpha = 1/3$ and $\alpha = 1/2$ is also shown.

to the error in the approximate moments calculation from the received signal samples as explained in section 2.5.1.2. It can also be seen that the EM estimator without noise

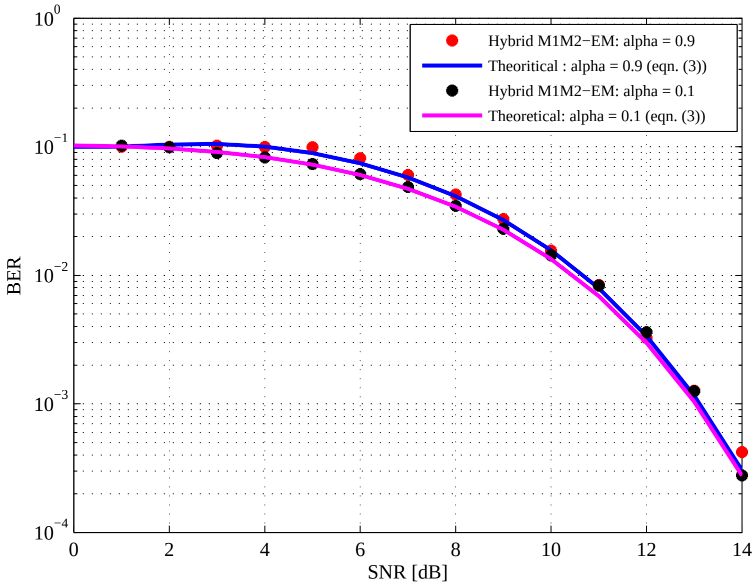

Figure 2.19: BER versus SNR [dB] for $M_1M_2 - EM$ NDA estimator for $\alpha = 0.1$ and $\alpha = 0.9$. $N = 512$ bits for all the cases Theoretical BER versus SNR [dB] for $\alpha = 0.1$ and $\alpha = 0.9$ is also shown.

recalibration has a significant bias. After recalibration, the NMSE of EM estimator has reduced significantly.

Figure 2.15 shows the mean SNR estimates of M_2M_3, EM and $M_2M_3 - EM$ hybrid estimators. It is evident from figure 2.14 and figure 2.15 that the hybrid $M_2M_3 - EM$ estimator overcomes the limitations of the individual estimators and gives the optimal performance.

Figure 2.16 shows the NMSE of M_1M_2, EM and $M_1M_2 - EM$ estimators for $\alpha = 1/3$. The performance of M_1M_2 estimator degrades for SNR$>$ 7 dB. The same argument of M_2M_3 estimator is valid here. The threshold, ρ_0, is set to 7 dB for the $M_1M_2 - EM$ hybrid estimator. The mean SNR estimates of the M_1M_2, EM and $M_1M_2 - EM$ estimators are shown in figure 2.17 and it is clear that the estimates of hybrid $M_1M_2 - EM$ estimator are close to the true SNR.

2.6 BER performance of SNR estimators

The BER performance of the M_1V and hybrid NDA estimators is determined by Monte Carlo simulation of 5000 iterations. The detection threshold is calculated from estimated SNR. The expression for theoretical BER is given in (2.11). Figure 2.18 shows the BER performance of M_1V DA estimator for $\alpha = 1/2$ and hybrid NDA estimators for $\alpha = 1/2$ and $\alpha = 1/3$. It is evident that the simulation is in good agreement with the analytically evaluated BER. The BER performance for extreme cases of $\alpha = 0.1$ and $\alpha = 0.9$ is shown in figure 2.19 and is found to be in good agreement with the analytically evaluated BER. Thus the proposed estimators are consistent over a wide range of α.

2.7 Summary

The NML method is proposed for non-coherent detection of OOK signals. The BER performance of NML detection was compared against the ML based non-coherent detection and it is found that the NML detection improves the BER performance and there is a gain of 1 dB at 2×10^{-4} BER for $\alpha = 0.3$. It is also shown that the gain decreases as α increases and there is a gain of 0.6 dB for equiprobable symbol condition and the gain reduces further to 0.3 dB for $\alpha = 0.7$. As the detection requires the knowledge of SNR, DA and NDA SNR estimation techniques are investigated for non-coherent detection of OOK signals. ML estimator, EM estimator and moments based estimators are proposed for SNR estimation. The NMSE performance of each estimator is evaluated over a wide range of SNR and the limitations are discussed. It is shown that M_1M_2 NDA estimator cannot be used in equiprobable case. Hence, M_2M_3 estimator is proposed for the equiprobable case. It is shown that the performance of moments based NDA estimators degrade in the high SNR region. Hence, EM estimator is proposed to overcome the problem at high SNR. It is also shown that the performance of moments based NDA estimators is better than EM estimator in the low SNR region. Hence, optimal hybrid $M_1M_2 - EM$ and $M_2M_3 - EM$ NDA estimators are also proposed to overcome the limitations. Finally, BER performance of the M_1V DA and hybrid NDA estimators is simulated and found to be in good agreement with the analytically evaluated BER. As, it will be seen in the subsequent chapters, the proposed DA and NDA SNR estimation techniques will be used for interference mitigation in the non-coherent OOK based wakeup radio receiver.

Interference mitigation techniques for wakeup radio

3

3.1 Introduction

Interference degrades the performance of wireless communication systems. The effect is even more profound in low power radios such as the wakeup radio because there is higher chance for interference power to be greater than the desired signal power. Therefore, it is necessary to develop interference mitigation techniques to enhance the detection performance of the wakeup radio in the presence of co-channel interference (CCI).

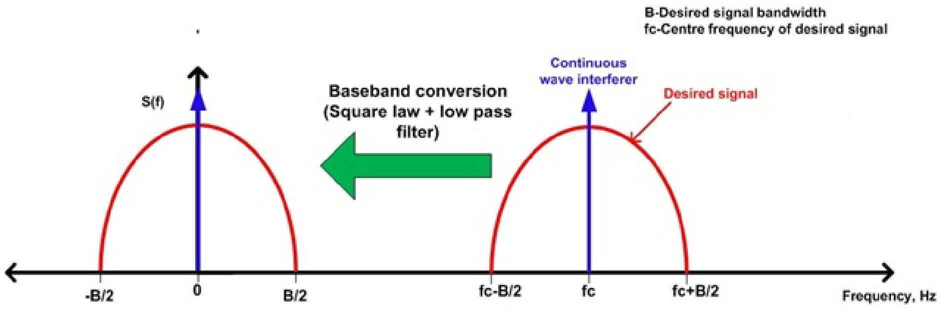

Figure 3.1: Illustration of the down conversion of the carrier to baseband and ignores the signal changes (i.e., amplitude etc.) due to the squaring (nonlinear) operation.

In this chapter, the continuous wave (CW) CCI and interference from on-off keying (OOK) modulated interferer are considered and mitigation techniques are proposed for both the cases. The effect of the CW-CCI on the desired signal is illustrated in figure 3.1. As it can be seen in the figure, the baseband signal is corrupted by the CCI and appropriate interference mitigation techniques have to be implemented in the digital baseband to enhance detection performance.

Various interference mitigation techniques are proposed in the literature, [5–11]. These techniques are not suitable for the wakeup radio receiver due to the certain system constraints. The system constraints imposed by the wakeup radio architecture are listed below.

- *Single RF chain*
  The low power requirements also limit the receiver to have only a single RF chain. Consequently, the receiver is equipped only with a single antenna. So the interference mitigation technique can't take advantage of source separation or other spatial processing techniques [7].

- *Analog front end*
  The analog front end of the wakeup radio receiver has been designed in accordance with the ultra low power requirement and it uses a square law detector to

convert RF to baseband. Due to the non-coherent operation, the phases of the desired and interfering signals are not completely preserved. The existing single antenna interference cancellation algorithms are suitable in the absence of multiple antennas, [10, 11] and the references therein. But, these techniques cannot be implemented for our case due to the non-coherent OOK reception.

- *Lower C/I ratio*
  As already mentioned, wakeup radio is an ultra low power (ULP) radio. Hence, the interference mitigation techniques must be suitable for lower carrier to interference ratio ($C/I < 0$ dB). The C/I ratio can be mathematically expressed as,

$$\frac{C}{I} = \frac{A^2}{I^2}, \tag{3.1}$$

  where, A and I are the amplitudes of desired and interfering signals, respectively.

The above constraints must be taken into account while proposing the appropriate interference mitigation techniques. These constraints also impose certain limitations on the efficiency of the mitigation techniques which will be discussed later in the chapter. Therefore, novel interference mitigation techniques are proposed for non-coherent OOK based systems in this chapter. At first, the techniques to estimate the interference, signal and noise power are discussed for the case of both CW and OOK modulated interferers. In the case of CW interferer, the data aided (DA) estimation techniques discussed in chapter 2 are extended to estimate the interference power along with the signal and noise power. The non data aided (NDA) estimation techniques are used in the case of OOK modulated interferer. Based on the estimates, two techniques are proposed for interference mitigation. The first one is based on maximum-a-posteriori (MAP) detection and the second one is based on threshold adjustment. It is to be noted that the interference is not cancelled in these techniques, but the interference effect is taken into account in both the threshold based and MAP detection schemes.

Finally, the bit error rate (BER) performance is evaluated after interference mitigation and is compared against the analytically evaluated BER of non-coherent OOK receiver. In the case of CW interferer, both the techniques have similar BER performance and are found to successfully mitigate the interference for $C/I \geq 0$ dB and $C/I < 0$ dB. In the case of OOK modulated interferer, the threshold based technique is only suitable for $C/I \geq 0$ dB whereas, the MAP detection is suitable for both $C/I > 0$ dB and $C/I \leq 0$ dB. It is also shown that the joint detection of interfering and desired signal is possible using MAP detection for the case of OOK modulated interferer.

The rest of the chapter is organized as follows. Section 3.2 describes the system model. Section 3.3 describes the signal, interference and noise power estimation for CW and OOK modulated interference cases. Section 3.4 describes the threshold based CW and OOK interference mitigation. Section 3.5 describes the MAP detector based CW and OOK interference mitigation. Section 3.6 describes the problems of the proposed techniques and the summary is presented in section 3.7.

3.2 System model

Figure 3.2 shows the simplified model of non-coherent OOK receiver with interference mitigation. The estimation is divided into two blocks. At first, the noise and interference power are estimated and then the signal power is estimated. The decision threshold is based on these estimates. The threshold derivations for CW and OOK modulated interferers are described in section 3.4.

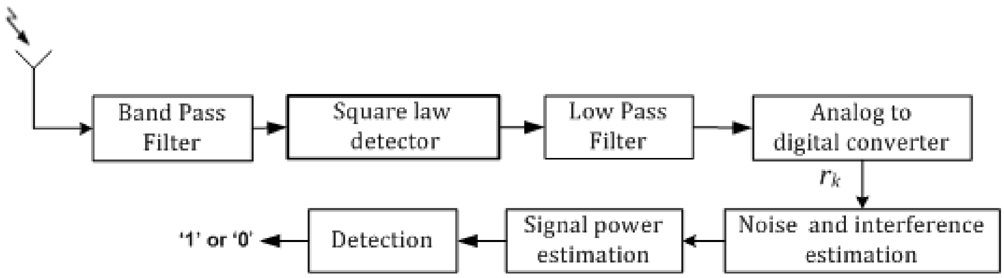

Figure 3.2: Simplified model of non-coherent OOK receiver with interference mitigation.

Consider the received packet structure shown in figure 3.3. This is similar to the packet structure mentioned in figure 2.2 except that the preamble has both zeros and ones. In the presence of CW interference of the form, $Icos(\omega t)$, the superposition of

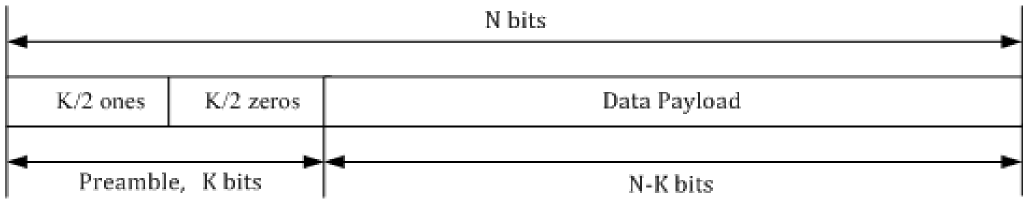

Figure 3.3: The data packet structure with K preamble bits and $N-K$ payload bits.

the interfering signal on the desired signal, $Ac_kcos(\omega t)$, results in the baseband signal,

$$r_k \quad = \quad (Ac_k + I + x_k)^2 + y_k^2, \qquad k = 0...N-1, \tag{3.2}$$

where, $c_k \in \{0, 1\}$ represents the transmitted binary sequence of the desired signal as mentioned before. In the presence of OOK modulated interferer of the form, $Id_kcos(\omega t)$, the superposition of the OOK interferer on the desired signal, results in the baseband signal,

$$r_k \quad = \quad (Ac_k + Id_k + x_k)^2 + y_k^2, \qquad k = 0...N-1, \tag{3.3}$$

where, $d_k \in \{0, 1\}$ represent the transmitted binary sequence of the OOK modulated interfering source. Let δ be the probability of '$d_k = 1$' and $1-\delta$ be the probability of '$d_k = 0$'. The conditional pdfs of r_k in the case of CW interferer are given by,

$$p_{cw}(r_k|c_k = 1) \quad = \quad \frac{1}{2\sigma^2} e^{-\frac{r_k + (A+I)^2}{2\sigma^2}} I_0\left(\frac{\sqrt{r_k}(A+I)}{\sigma^2}\right), \tag{3.4}$$

$$p_{cw}(r_k|c_k = 0) \quad = \quad \frac{1}{2\sigma^2} e^{-\frac{r_k + I^2}{2\sigma^2}} I_0\left(\frac{\sqrt{r_k} I}{\sigma^2}\right). \tag{3.5}$$

In the case of OOK interferer, the interfering signal may or may not be present conditioned on the parameter d_k. This results in the following four conditional pdfs of r_k in the case of OOK interferer.

$$
\begin{aligned}
p_{ook}(r_k|'c_k = 1 \text{ and } d_k = 1') &= \frac{1}{2\sigma^2} e^{-\frac{r_k+(A+I)^2}{2\sigma^2}} I_0\left(\frac{\sqrt{r_k}(A+I)}{\sigma^2}\right), && (3.6)\\
p_{ook}(r_k|'c_k = 1 \text{ and } d_k = 0') &= \frac{1}{2\sigma^2} e^{-\frac{r_k+A^2}{2\sigma^2}} I_0\left(\frac{\sqrt{r_k}A}{\sigma^2}\right), && (3.7)\\
p_{ook}(r_k|'c_k = 0 \text{ and } d_k = 1') &= \frac{1}{2\sigma^2} e^{-\frac{r_k+I^2}{2\sigma^2}} I_0\left(\frac{\sqrt{r_k}I}{\sigma^2}\right), && (3.8)\\
p_{ook}(r_k|'c_k = 0 \text{ and } d_k = 0') &= \frac{1}{2\sigma^2} e^{-\frac{r_k}{2\sigma^2}}. && (3.9)
\end{aligned}
$$

It is to be noted that we have used the subscripts *cw* and *ook* in the pdfs to identify the source of interference. It is different from the standard mathematical notations of the pdf where the subscript usually represents the random process corresponding to the random variable described by the pdfs.

In the following section, the estimation techniques are described in detail for both CW and OOK modulated interferers.

3.3 Estimation of parameters

3.3.1 Case 1: CW interference

Consider the data packet structure as shown in figure 3.3. We assume there are equal number of ones and zeros in the preamble. Let, R_{1K} and R_{0K} represent the vectors of baseband signal samples corresponding to the ones and zeros in the preamble, respectively. The elements of R_{0K} are affected by the amplitude of the CW interferer as mentioned in (3.2). The elements of R_{1K} are affected by the superposition of CW interference on the desired signal. The pdfs of the elements of R_{0K} and R_{1K} are given by (3.5) and (3.4), respectively. Let, μ_0^1 and V_0 be the true first moment and variance of the elements of R_{0K}, respectively. They are given as [refer section 2.4.2],

$$
\begin{aligned}
\mu_0^1 &= 2\sigma^2 + I^2, && (3.10)\\
V_0 &= 4\sigma^4 + 4\sigma^2 I^2. && (3.11)
\end{aligned}
$$

Let μ_1^1 be the true first moment of the elements of R_{1K}.

$$
\mu_1^1 = 2\sigma^2 + (A+I)^2, \quad (3.12)
$$

The approximate moments are obtained as given in (2.25). At first, the interference and noise power are estimated from the elements of R_{0K} by solving (3.10) and (3.11).

The estimates are given by,

$$\hat{I}^2 = \sqrt{\hat{\mu_0^1}^2 - V_0}, \tag{3.13}$$

$$2\hat{\sigma}^2 = \hat{\mu_0^1} - \sqrt{\hat{\mu_0^1}^2 - V_0}. \tag{3.14}$$

Substituting (3.14) in (3.12) gives,

$$(\hat{A} + \hat{I})^2 = \hat{\mu_1^1} - 2\hat{\sigma}^2. \tag{3.15}$$

3.3.2 Case 2: OOK modulated interference

Consider the data packet structure shown in figure 3.3. The estimation procedure involves two steps.

- *Interference and noise power estimation*
  The interference and noise power are estimated from the elements of R_{0K}. In the case of CW interferer, M_1V DA estimation technique was used to estimate these parameters. In the case of OOK modulated interferer, it is not possible to use the DA estimation technique as the interferer is not always present in the elements of R_{0K}. Hence, the expectation maximization (EM) NDA estimator is used. The moments based NDA estimators are not used because they require relatively more baseband samples whereas, the number of elements in R_{0K} can be only as large as the preamble length.

- *Signal power estimation*
  Once the interference and noise power are estimated, the signal power can be estimated either from the elements of R_{1K} or from the baseband samples corresponding to the data payload.

The above steps are explained in detail in the following sections.

3.3.2.1 Interference and noise power estimation

The joint pdf of the elements of R_{0K} conditioned on the vector of OOK interference symbols, D_K, is given by,

$$p(R_{0K}|D_K) = \prod_{k=J}^{K-1} \frac{1}{2\sigma^2} e^{-\frac{r_k + I^2 d_k^2}{2\sigma^2}} I_0\Big(\frac{\sqrt{r_k} I d_k}{\sigma^2}\Big),$$

where, $J = K/2$ is the number of the zeros in the preamble. Since the zeros in the preamble start from $(K/2)^{th}$ symbol in the preamble, the subscript start from $k = J$. The EM estimation is performed based on the above pdf. The expectation is taken with respect to the parameter $d_k \in D_K$. Here, we give only the expressions for the estimates [Refer to section 2.5.2 for detailed procedure]. The estimates of interference power and noise power at the end of n^{th} iteration of the EM algorithm are given by,

$$
\begin{aligned}
I_n &= \frac{\sum_{k=J}^{K-1} P^d_{1k,n-1}\sqrt{r_k}}{\sum_{k=J}^{K-1} P^d_{1k,n-1}}, && (3.16)\\
2\sigma_n^2 &= \frac{1}{J}\left[\sum_{k=J}^{K-1} r_k - I_n^2 \sum_{k=J}^{K-1} P^d_{1k,n-1}\right], && (3.17)
\end{aligned}
$$

where,

$$
\begin{aligned}
P^d_{ik,n-1} &= P(d_k = i|r_k; I_{n-1}, \sigma_{n-1}), \qquad i = 0, 1,\\
&= \frac{P(r_k|d_k = i; I_{n-1}, \sigma_{n-1})P^d_i}{P(r_k; A_{n-1}, \sigma_{n-1})},
\end{aligned}
$$

where,

$$
\begin{aligned}
P^d_i &= \begin{cases} \delta, & \text{if } i = 1,\\ 1-\delta, & \text{if } i = 0, \end{cases}\\
P(r_k|d_k = i; I_{n-1}, \sigma_{n-1}) &= \frac{1}{2\sigma^2_{n-1}} e^{-\frac{r_k + I^2_{n-1} i^2}{2\sigma^2_{n-1}}} I_0\Big(\frac{\sqrt{r_k} I_{n-1} i}{\sigma^2_{n-1}}\Big),\\
P(r_k; I_{n-1}, \sigma_{n-1}) &= \sum_{i=0}^{1} P(r_k|d_k = i; I_{n-1}, \sigma_{n-1})P^d_i.
\end{aligned}
$$

After noise recalibration, the noise estimate is given by,

$$
2\sigma_n^2 = \frac{\sum_{k=J}^{K-1} P^d_{0k,n} r_k}{\sum_{k=J}^{K-1} P^d_{0k,n}}. \tag{3.18}
$$

where,

$$
P^d_{0k,n} \approx \begin{cases} 1, & \text{if } d_k = 0,\\ 0, & \text{if } d_k = 1. \end{cases}
$$

3.3.2.2 Signal power estimation

The signal power can be estimated by EM estimation or moments based estimation. The following sections explain both these techniques.

EM based signal power estimation
EM based signal power estimation is done from the elements of R_{1K}. The joint pdf of the elements of R_{1K} conditioned on the vector of OOK interference symbols, D_K, is given by,

$$
p(R_{1K}|D_K) = \prod_{k=0}^{J-1} \frac{1}{2\sigma^2} e^{-\frac{r_k + (A + I d_k)^2}{2\sigma^2}} I_0\Big(\frac{\sqrt{r_k}(A + I d_k)}{\sigma^2}\Big),
$$

where, $J = K/2$ is the number of ones in the preamble. The log likelihood of $p(R_{1K}|D_K)$ is given as,

$$\Lambda_{EM}(R_{1K};A;I;\sigma^2) = -Jln(2\sigma^2) - \frac{1}{2\sigma^2}\left[\sum_{k=0}^{J-1} r_k + JA^2 + I^2\sum_{k=0}^{J-1} d_k^2 + 2AI\sum_{k=0}^{J-1} d_k\right] + \sum_{k=0}^{J-1} ln\left(I_0\Big(\frac{\sqrt{r_k}(A+Id_k)}{\sigma^2}\Big)\right).$$

The expectation of $\Lambda_{EM}(R_{1K};A;I;\sigma^2)$, taken with respect to the parameter d_k is given by,

$$\begin{aligned}\Psi(R_{1K};A;I;\sigma^2) &= -Jln(2\sigma^2) - \frac{1}{2\sigma^2}\left[\sum_{k=0}^{J-1} r_k + JA^2 + I^2\sum_{k=0}^{J-1} P^d_{1k,n-1} + 2AI\sum_{k=0}^{J-1} P^d_{1k,n-1}\right] \\ &+ \sum_{k=0}^{J-1} P^d_{1k,n-1} ln\left(I_0\Big(\frac{\sqrt{r_k}(A+Id_k)}{\sigma^2}\Big)\right) \\ &+ \sum_{k=0}^{J-1} P^d_{0k,n-1} ln\left(I_0\Big(\frac{\sqrt{r_k}A}{\sigma^2}\Big)\right).\end{aligned} \quad (3.19)$$

Partially differentiating (3.19) with respect to A,

$$\begin{aligned}\frac{\partial\Psi(R_{1K};A;I;\sigma^2)}{\partial A} &= -\frac{1}{\sigma^2}[JA + I\sum_{k=0}^{J-1} P^d_{1k,n-1}] + \sum_{k=0}^{J-1} P^d_{1k,n-1}\frac{I_1\Big(\frac{\sqrt{r_k}(A+I)}{\sigma^2}\Big)}{I_0\Big(\frac{\sqrt{r_k}(A+I)}{\sigma^2}\Big)}\frac{\sqrt{r_k}}{\sigma^2} \\ &+ \sum_{k=0}^{J-1} P^d_{0k,n-1}\frac{I_1\Big(\frac{\sqrt{r_k}A}{\sigma^2}\Big)}{I_0\Big(\frac{\sqrt{r_k}A}{\sigma^2}\Big)}\frac{\sqrt{r_k}}{\sigma^2}.\end{aligned} \quad (3.20)$$

The estimate of A at the end of n^{th} iteration (A_n) is obtained by equating (3.20) to 0. After high SNR approximation, A_n is given by,

$$A_n = \frac{\sum_{k=0}^{J-1}(P^d_{0k,n-1} + P^d_{1k,n-1})\sqrt{r_k} - I\sum_{k=0}^{J-1} P^d_{1k,n-1}}{J}. \quad (3.21)$$

Since, the interference and noise power are estimated before, the estimate A_n can be obtained. The other method to obtain the signal power is using moments based estimators on the data payload. Since the number of samples is more on the data payload, the moments based estimators give good estimates. The moments based signal power estimator is explained in the following section.

Moments based signal power estimation

The pdf of r_k corresponding to the data payload is given by,

$$\begin{aligned} p_{ook}(r_k) &= p_{ook}(r_k|'c_k = 1 \text{ and } d_k = 1')\delta\alpha + p_{ook}(r_k|'c_k = 1 \text{ and } d_k = 0')(1-\delta)\alpha \\ &\quad + p_{ook}(r_k|'c_k = 0 \text{ and } d_k = 1')(1-\alpha)\delta \\ &\quad + p_{ook}(r_k|'c_k = 0 \text{ and } d_k = 0')(1-\delta)(1-\alpha). \end{aligned} \tag{3.22}$$

Let, R_{data} represent the vector of baseband signal samples corresponding to the data payload in the packet structure shown in figure 3.3. The true first moment (μ^1_{data}) of the elements of R_{data} corresponding to the pdf described in (3.22) is given by,

$$\begin{aligned} \mu^1_{data} &= \delta\alpha(2\sigma^2 + (A+I)^2) + \alpha(1-\delta)(2\sigma^2 + A^2), \\ &\quad + \delta(1-\alpha)(2\sigma^2 + I^2) + (1-\delta)(1-\alpha)2\sigma^2. \end{aligned} \tag{3.23}$$

Assuming equiprobable symbol conditions for both the desired signal and the interfering signal ($\alpha = \delta = 0.5$), (3.23) can be simplified as,

$$2\mu^1_{data} = 4\sigma^2 + I^2 + AI + A^2.$$

Solving the above equation yields the expression for A as,

$$A = \frac{\sqrt{I^2 - 4(4\sigma^2 + I^2 - 2\mu^1_{data})} - I}{2} \tag{3.24}$$

μ^1_{data} is obtained from the received baseband signal samples as given in (2.25).

Based on the estimates, the threshold and MAP detection based interference mitigation techniques are proposed. In the following section, the threshold based interference mitigation is described in detail for both CW and OOK modulated interference.

3.4 Threshold based interference mitigation

3.4.1 Case 1: CW interference

The optimal decision threshold (b_0) is chosen such that it minimizes the probability of error. The probability of Mark error (P_m), Space error (P_s) and the overall probability of error (P_e) in the presence of CW interferer are derived as follows.

$$\begin{aligned} P_m &= 1 - \int_{b_0}^{\infty} p_{cw}(r_k|c_k = 1) \;\; dr_k, \\ &= 1 - \int_{b_0}^{\infty} \frac{1}{2\sigma^2} e^{-\frac{r_k + (A+I)^2}{2\sigma^2}} I_0\Big(\frac{\sqrt{r_k}(A+I)}{\sigma^2}\Big) \;\; dr_k, \\ P_s &= \int_{b_0}^{\infty} p_{cw}(r_k|c_k = 0) \;\; dr_k, \\ &= \int_{b_0}^{\infty} \frac{1}{2\sigma^2} e^{-\frac{r_k + I^2}{2\sigma^2}} I_0\Big(\frac{\sqrt{r_k} I}{\sigma^2}\Big) \;\; dr_k. \end{aligned}$$

Similar to section 2.2, the above equations are simplified by the following transformations.

$$\begin{aligned} r_n^2 &= \frac{r_k}{\sigma^2}, \\ \varphi &= \frac{(A+I)^2}{2\sigma^2}, \\ \eta &= \frac{I^2}{2\sigma^2}, \\ \beta &= \frac{\sqrt{b_0}}{\sigma}. \end{aligned} \tag{3.25}$$

Then,

$$\begin{aligned} P_m &= 1 - \int_{\beta}^{\infty} r_n e^{-\frac{r_n^2 + (\sqrt{2\varphi})^2}{2}} I_0\Big(r_n \sqrt{2\varphi}\Big) \;\; dr_n, \\ &= 1 - Q(\sqrt{2\varphi}, \beta), \\ P_s &= \int_{\beta}^{\infty} r_n e^{-\frac{r_n^2 + (\sqrt{2\eta})^2}{2}} I_0\Big(r_n \sqrt{2\eta}\Big) \;\; dr_n, \\ &= Q(\sqrt{2\eta}, \beta), \\ P_e &= \alpha P_m + (1-\alpha) P_s, \end{aligned} \tag{3.26}$$

β must be chosen such that it minimizes P_e. This is done by partially differentiating P_e with respect to β and equating to 0 as shown below.

$$\begin{aligned} \alpha \frac{\partial P_m}{\partial \beta} + (1-\alpha) \frac{\partial P_s}{\partial \beta} &= 0, \\ -\alpha \frac{\partial (Q(\sqrt{2\varphi}, \beta))}{\partial \beta} + (1-\alpha) \frac{\partial (Q(\sqrt{2\eta}, \beta))}{\partial \beta} &= 0, \end{aligned} \tag{3.27}$$

where, $\frac{\partial (Q(a,b))}{\partial b} = b e^{\frac{-(a^2+b^2)}{2}} I_0(ab)$. Upon simplifying,

$$\alpha \beta e^{\frac{-(2\varphi + \beta^2)}{2}} I_0(\sqrt{2\varphi}\beta) = (1-\alpha) \beta e^{\frac{-(2\eta + \beta^2)}{2}} I_0(\sqrt{2\eta}\beta). \tag{3.28}$$

Approximating $I_0(x) \approx e^x/\sqrt{2\pi x}$ for $x >> 1$, (3.28) can be rewritten as,

$$\begin{aligned} e^{\frac{-(2\varphi+\beta^2)}{2}} \frac{e^{\sqrt{2\varphi}\beta}}{\sqrt{2\pi\sqrt{2\varphi}\beta}} &= \frac{(1-\alpha)e^{\frac{-(2\eta+\beta^2)}{2}} e^{\sqrt{2\eta}\beta}}{\alpha\sqrt{2\pi\sqrt{2\eta}\beta}}, \\ e^{\beta\sqrt{2}(\sqrt{\varphi}-\sqrt{\eta})} &= \frac{(1-\alpha)}{\alpha} e^{(\varphi-\eta)} \left(\frac{\sqrt{\varphi}}{\sqrt{\eta}}\right)^{1/2}. \end{aligned} \tag{3.29}$$

Taking logarithm on both sides of (3.29) gives,

$$\beta = \frac{ln\left[\frac{(1-\alpha)}{\alpha}\left(\frac{\sqrt{\varphi}}{\sqrt{\eta}}\right)^{1/2}\right] + (\varphi - \eta)}{\sqrt{2}(\sqrt{\varphi}-\sqrt{\eta})}. \tag{3.30}$$

(3.30) gives the solution for the optimum normalized threshold, β, for the case of CW interferer. φ and η can be estimated from (3.13), (3.14) and (3.15). The CW interference can be mitigated once the detection threshold b_0 is set to $(\beta\sigma)^2$ as mentioned in (3.25).

In the following section, BER performance of the threshold based CW interference mitigation technique is explained in detail.

3.4.1.1 BER performance of threshold based CW interference mitigation

Figure 3.4 shows the BER performance of the threshold based CW interference mitigation technique for different C/I values based on the true values of signal, interference and noise power respectively. The preamble length, $K = 32$ bits and packet length $N = 512$ bits for all cases. The BER performance is plotted after 500 Monte Carlo simulation runs. It is evident that that the threshold based technique is effective in mitigating the interference. Moreover, the performance is improved in the presence of interference as the relative spacing between zero and one increases in the presence of CW interference and there is a gain of 1 dB at 2.5×10^{-2} BER. This can be explained from figure 3.6 and figure 3.7. Figure 3.6 shows the pdfs $p(r_k|c_k = 1)$ and $p(r_k|c_k = 0)$ in the absence of CW interference signal for SNR = 10 dB. Figure 3.7 shows the pdfs $p(r_k|c_k = 1)$ and $p(r_k|c_k = 0)$ in the presence of CW interference for SNR = 10 dB and $C/I = 0$ dB. The region of error of the pdfs is more in the absence of interference when compared to the presence of interference. Thus the decision region is more pronounced in the presence of interference, leading to improved performance.

The BER performance without interference mitigation is also shown in figure 3.4. It is evident that without interference mitigation, it is not possible to have reliable detection performance. Figure 3.5 shows the BER performance of the threshold based CW interference mitigation technique for different C/I values based on the estimated values of signal, interference and noise power respectively and it is in close agreement with figure 3.4.

In the following section, threshold based interference mitigation technique for OOK modulated interferer is discussed in detail.

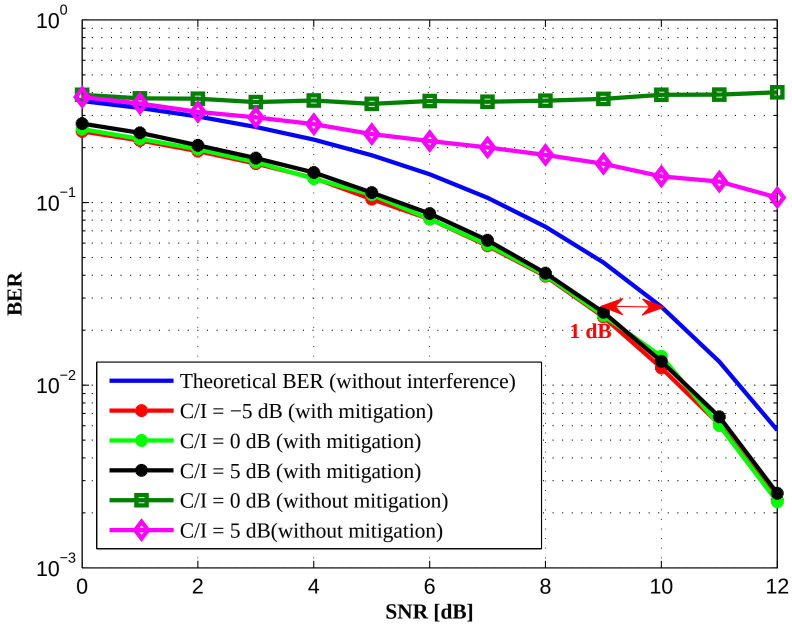

Figure 3.4: Comparison of BER performance of threshold based CW interference mitigation based on the true values of signal, interference and noise power against the theoretical BER performance of non-coherent OOK receiver for different C/I values. The BER performance without mitigation is also shown. Preamble length, $K = 32$ bits and total packet length, $N = 512$ bits.

3.4.2 Case 2: OOK modulated interference

Consider the OOK modulated interferer as described in section 3.2. The received baseband signal is given by (3.3). The detection criterion is based on the following four hypotheses.

$$\begin{aligned} H_0(c_k = 1, d_k = 1) : r_k &= (A + I + x_k)^2 + y_k^2, \\ H_1(c_k = 1, d_k = 0) : r_k &= (A + x_k)^2 + y_k^2, \\ H_2(c_k = 0, d_k = 1) : r_k &= (I + x_k)^2 + y_k^2, \\ H_3(c_k = 0, d_k = 0) : r_k &= x_k^2 + y_k^2. \end{aligned}$$

The threshold based OOK interference mitigation technique can be used to detect the desired signal when the interferer is less than the desired signal, i.e, for the case of $C/I > 0$ dB. In this case, it is enough to find a single threshold between the received baseband signal amplitude levels of H_1 and H_2. The procedure is similar to the one followed in CW interferer case. The expression for the OOK threshold is also similar to the CW threshold (3.30), except a slight modification. φ is replaced by $\rho = \frac{A^2}{2\sigma^2}$ and the prior probabilities are replaced correspondingly. The threshold, (β_{ook}) is given by,

$$\beta_{ook} = \frac{ln\left[\frac{\delta(1-\alpha)}{\alpha(1-\delta)}\left(\frac{\sqrt{\rho}}{\sqrt{\eta}}\right)^{1/2}\right] + (\rho - \eta)}{\sqrt{2}(\sqrt{\rho} - \sqrt{\eta})}. \quad (3.31)$$

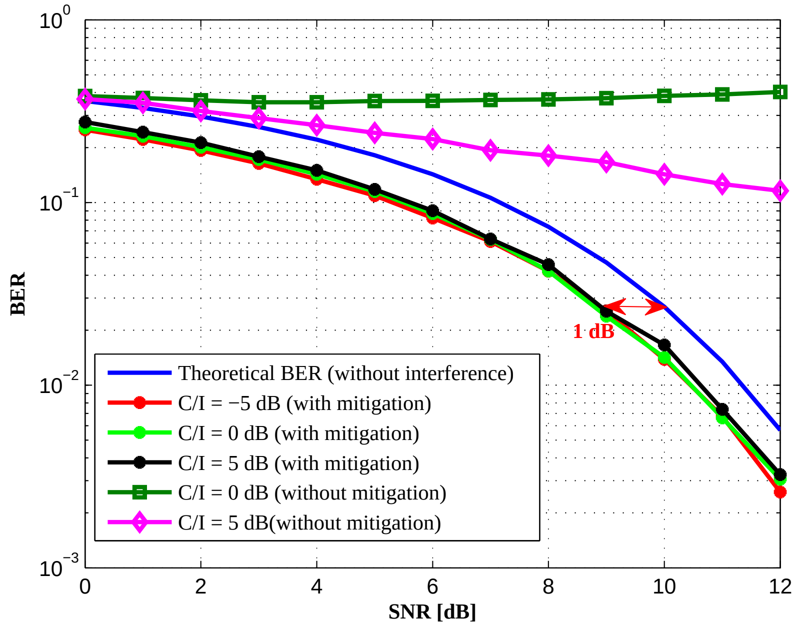

Figure 3.5: Comparison of BER performance of threshold based CW interference mitigation based on the estimated values of signal, interference and noise power against the theoretical BER performance of non-coherent OOK receiver for different C/I values. The BER performance without mitigation is also shown. Preamble length, $K = 32$ bits and total packet length, $N = 512$ bits.

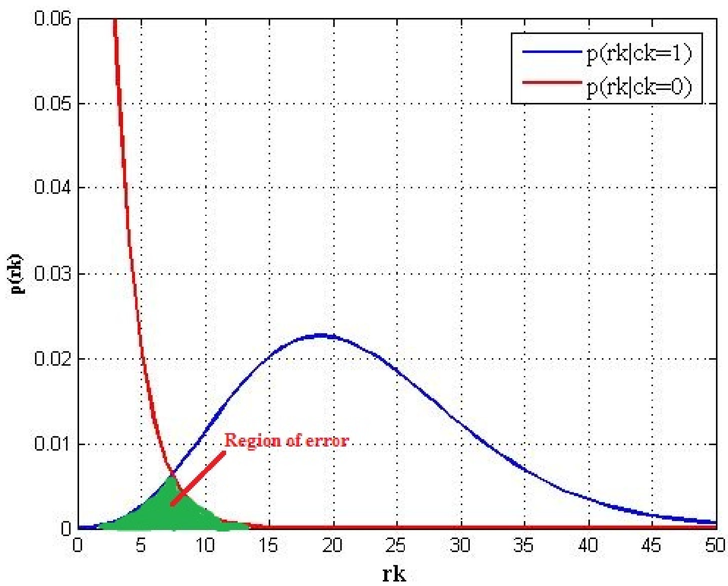

Figure 3.6: Plots of the pdf of r_k corresponding to '$c_k = 1$' and '$c_k = 0$' in the absence of interference.

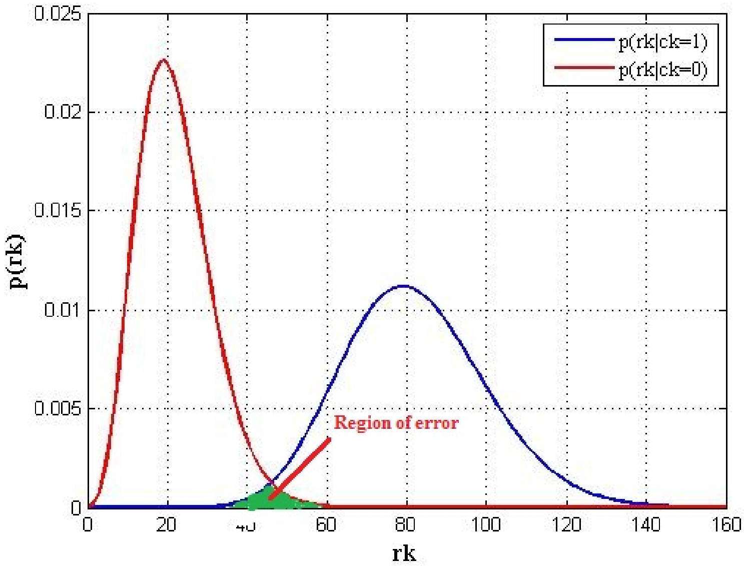

Figure 3.7: Plots of the pdf of r_k corresponding to '$c_k = 1$' and '$c_k = 0$' in the presence of interference for $SNR = 10$ dB and $C/I = 0$ dB.

In the following section, BER performance of threshold based interference mitigation of OOK modulated interferer is discussed in detail.

3.4.2.1 BER performance of threshold based OOK modulated interference mitigation

Figure 3.8 shows the BER performance of the threshold based OOK modulated interference mitigation method using the true signal, interference and noise power for different $C/I > 0$ dB. The BER performance without interference mitigation is also shown. It is evident that the threshold based method is able to mitigate the interference, though the performance is not as good as the CW interference mitigation. The limiting case is $C/I = 0$ dB where we would not be able to differentiate the hypothesis H_2 and H_1. Thus when C/I values moves away from 0 dB, the performance improves. Figure 3.9 shows the BER performance of the threshold based OOK interference mitigation method using the estimated signal, interference and noise power for different $C/I > 0$ dB and it is in close agreement with the figure 3.8.

In the following section, the MAP detector based interference mitigation is described in detail for CW and OOK modulated interference.

3.5 MAP detector based interference mitigation

Let H_d represent the output hypothesis after MAP detection. The MAP decision rule is given by,

$$H_d = \arg\max_{H_i}[p(r_k|H_i; A, I, \sigma^2)p(H_i)]. \qquad \text{for i=0,1,2,3.} \tag{3.32}$$

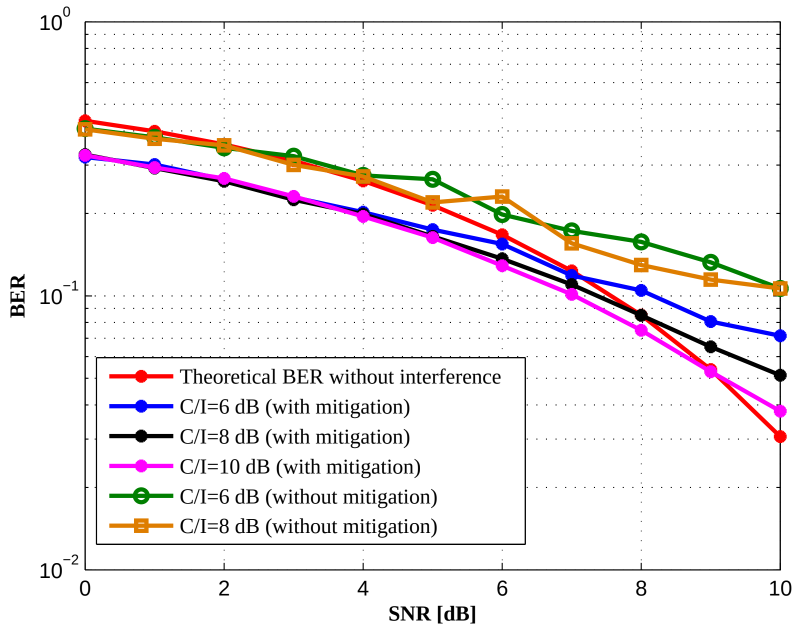

Figure 3.8: BER performance of threshold based OOK interference mitigation for different C/I values based on the true values of signal, interference and noise power. The packet length $N = 512$ bits and the preamble length $K = 32$ bits.

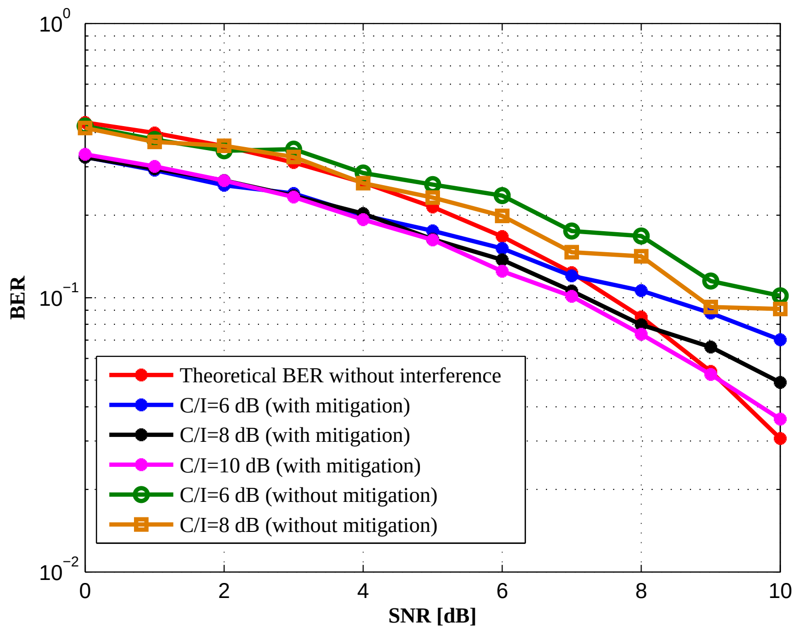

Figure 3.9: BER performance of threshold based OOK interference mitigation for different C/I values based on the estimated values of signal, interference and noise power. The packet length $N = 512$ bits and the preamble length $K = 32$ bits.

In the case of CW interferer, it is a binary hypotheses problem. So, $p(r_k|H_i)$ is given by (3.4) and (3.5) for CW interference. In the case of OOK modulated interference, we have four different hypotheses as described in section 3.4.2. So, $p(r_k|H_i)$ is given by (3.6), (3.7), (3.8) and (3.9) for OOK modulated interference.
Considering CW interference,

$$\begin{aligned} p(H_0) &= \alpha, \\ p(H_1) &= (1-\alpha). \end{aligned}$$

Considering OOK modulated interference,

$$\begin{aligned} p(H_0) &= \alpha\delta, \\ p(H_1) &= \alpha(1-\delta), \\ p(H_2) &= (1-\alpha)\delta, \\ p(H_3) &= (1-\alpha)(1-\delta). \end{aligned}$$

It is seen that the MAP detector requires the calculation of $p(r_k|H_i)$. Hence, the signal, interference and noise power has to be estimated as explained in section 3.3 for CW and OOK modulated interference. Once the estimates are obtained, the MAP detection is done using (3.32). In the presence of OOK modulated interference, the MAP detection performs the joint detection of both interfering and desired signals as explained below.

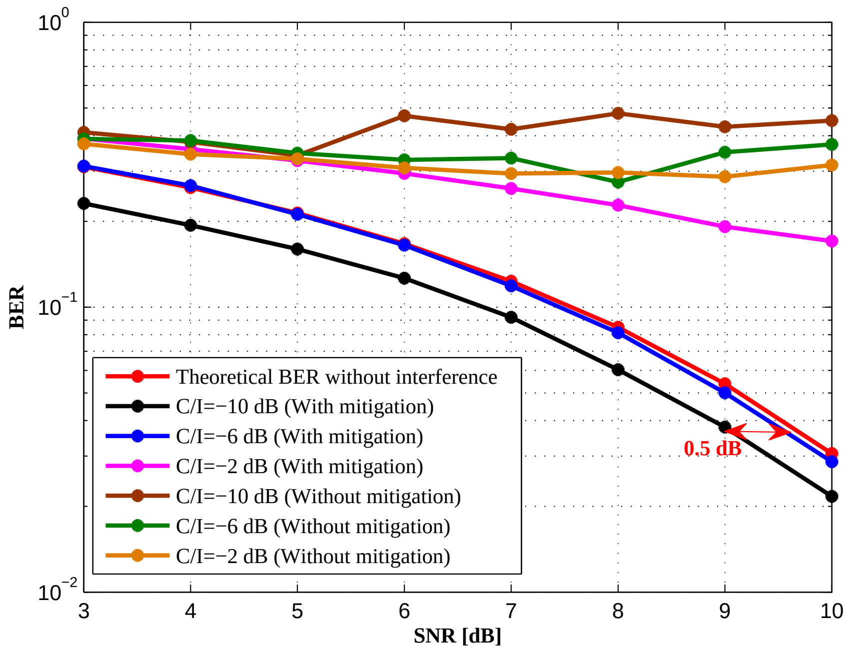

Figure 3.10: BER performance for MAP detection based OOK modulated interference mitigation using the true signal, interference and noise power for different $C/I <= 0$ dB. The packet length $N = 512$ bits and the preamble length $K = 32$ bits.

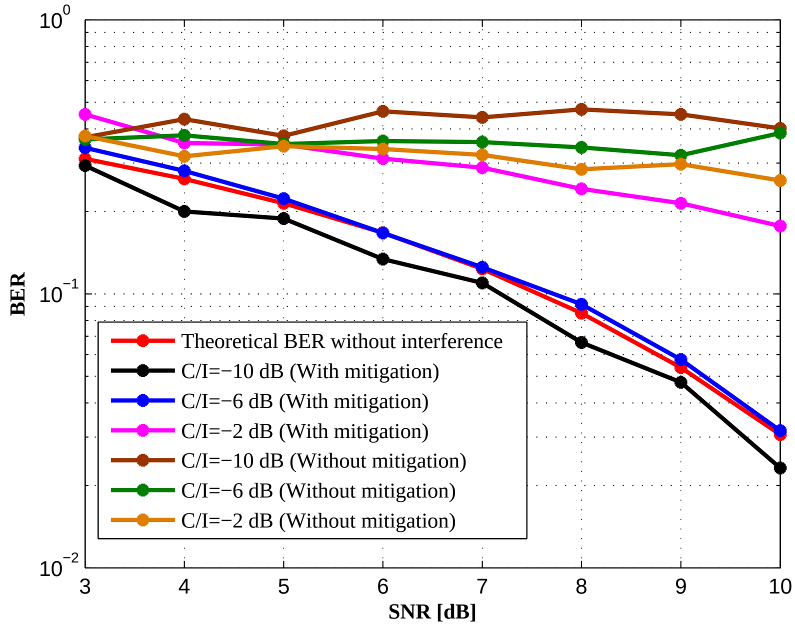

Figure 3.11: BER performance for MAP detection based OOK modulated interference mitigation using the estimated signal, interference and noise power for different $C/I <= 0$ dB. The packet length $N = 512$ bits and the preamble length $K = 32$ bits.

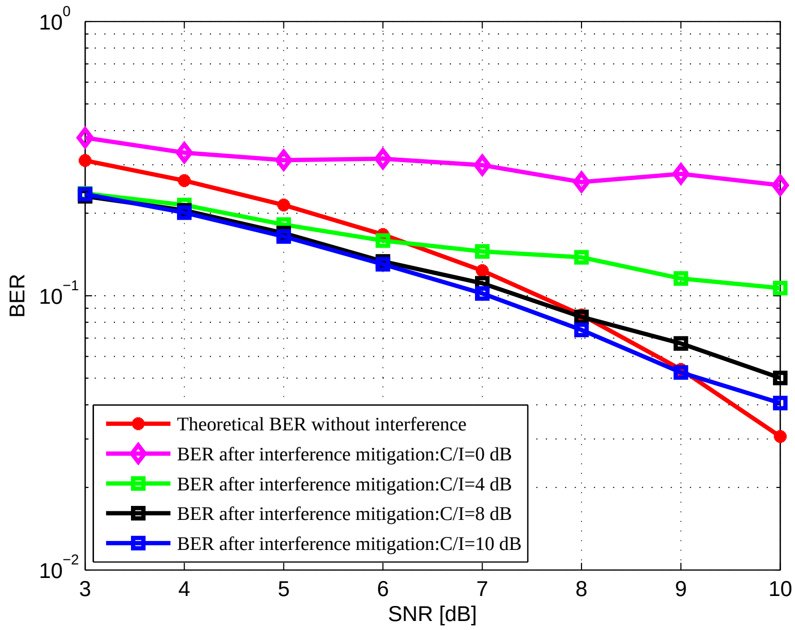

Figure 3.12: BER performance for MAP detection based OOK modulated interference mitigation using the true signal, interference and noise power for different $C/I \geq 0$ dB. The packet length $N = 512$ bits and the preamble length $K = 32$ bits.

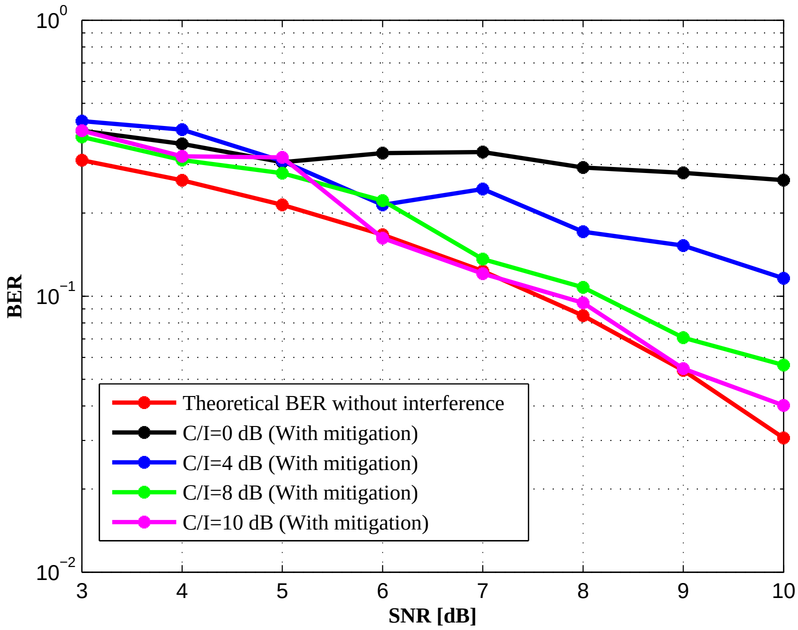

Figure 3.13: BER performance for MAP detection based OOK modulated interference mitigation using the estimated signal, interference and noise power for different $C/I \geq 0$ dB. The packet length $N = 512$ bits and the preamble length $K = 32$ bits,

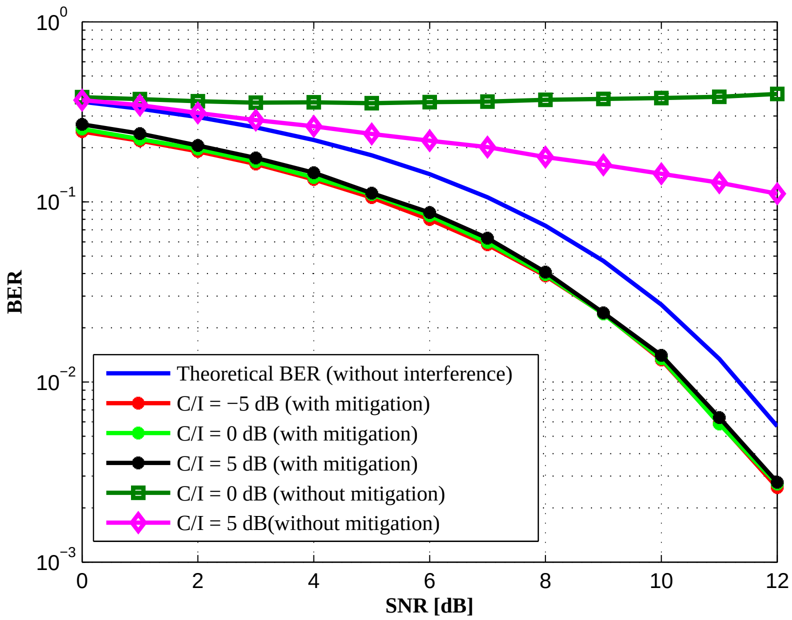

Figure 3.14: BER performance for MAP detection based CW interference mitigation for different C/I values. The packet length $N = 512$ bits and the preamble length $K = 32$ bits.

3.5.1 Joint detection

The MAP decision rule (3.32) is used to detect all the four hypotheses levels. Therefore, based on the detected hypothesis, we can determine the symbols of interfering and desired signals. The joint detection summary is depicted in table 3.1.

Table 3.1: Joint detection summary

Detected hypothesis	Interfering symbol (d_k)	desired symbol (c_k)
H_0	1	1
H_1	0	1
H_2	1	0
H_3	0	0

In the following section, the BER performance of MAP detection based interference mitigation is described in detail.

3.5.2 BER performance of MAP detection

Figure 3.10 show the BER performance of the desired signal by the MAP detection method for $C/I <= 0$ dB using the true signal, interference and noise power values. It can be seen that effective interference mitigation is possible for $C/I < 0$ dB and also the performance degrades when the C/I ratio moves towards the 0 dB mark. It can also be seen that for higher magnitude of C/I (ignoring the sign), the performance is better than the without interference case. The reason is same as the one described in CW interference mitigation case in section 3.4.1.1 and the improvement in this case is less than the CW interference case because the interfering signal is not always present leading to more ambiguity in the decision criteria. For example, for $C/I = -10$ dB, there is a gain of 0.5 dB at 3.7×10^{-2} BER. Figure 3.11 shows the same BER performance using the estimated signal, interference and noise power. It is clear that the BER performance using the estimates is close to that of using the true values.

Figure 3.12 shows the BER performance of the desired signal by the MAP detection method for $C/I >= 0$ dB using the true signal, interference and noise power values. It is shown that reliable detection is not possible at $C/I = 0$ dB. Similar to the previous case, the performance improves when the C/I values move away from the 0 dB mark. Figure 3.13 shows the same BER performance using the estimated signal, interference and noise power and is close to that of using the true values.

Figure 3.14 shows the BER performance of CW interference mitigation by MAP detection. The performance is same as the threshold based detection.

In the following section, the problems of the proposed techniques are explained briefly.

3.6 Problems of the proposed techniques

In the previous sections, the interference mitigation techniques for CW and OOK modulated interference were discussed in detail. In the case of $MPSK$ modulated interferes, the MAP detection will be complex as the phase of the interferer can change from one symbol to the next resulting in more hypothesis levels for MAP detection. The threshold based detection is also not possible as we would not be able to find a single optimal threshold. Hence, the proposed techniques are not suitable for $MPSK$ modulated interferers. During this thesis work, we have also proposed another technique for the case of $MPSK$ modulated interferers that can also be used for the case of CW interferers. Due to confidentiality reasons, that technique is not described in this report.

3.7 Summary

In this chapter, the interference mitigation techniques for CW and OOK modulated interferers are discussed in detail. Threshold based and MAP detection based interference mitigation is proposed for CW and OOK modulated interference. DA moments based method is proposed to estimate the interference, desired signal and noise power in the case of CW interference. NDA EM and moments based methods are proposed to estimate the interference, desired signal and noise power in the presence of OOK modulated interferer. The extension of MAP detection to the joint detection of interfering and desired signal for the OOK modulated interference case is also discussed. The BER performance of each of the proposed techniques is simulated and compared against the analytically evaluated BER. The limitations and the effectiveness of each of the proposed techniques are discussed in terms of the BER performance. It is shown that there is a gain of 1 dB at 2.5×10^{-2} BER after CW interference mitigation. It is shown for the case of OOK modulated interferer that the threshold based technique is suitable for $C/I > 0$ dB and the MAP detection is suitable for both $C/I \geq 0$ dB and $C/I < 0$ dB. It is also shown that the proposed techniques are not suitable to mitigate *MPSK* modulated interferers. In the forthcoming chapter, the implementation of the NDA estimation techniques in the real time hardware platform is discussed in detail.

4 Implementation of non data aided SNR estimation

4.1 Introduction

The main contributions of this thesis are signal to noise ratio (SNR) estimation and interference mitigation techniques. In previous chapters, the results from MATLAB simulations of the proposed techniques were presented. In the given time frame of this thesis work, we implemented the non data aided (NDA) SNR estimation techniques in the real time hardware platform. In this chapter, the implementation of NDA SNR estimation techniques in a real time hardware platform is discussed. The chosen hardware platform for receiver is the universal software radio peripheral 2 (USRP2). In the transmitter side, a Tektronix arbitrary/function generator (AFG3252) and Agilent E8257D signal generator is used to generate the on-off keying signal. Since the proposed estimation techniques considered only AWGN channel, we wanted to prevent any channel anomalies such as fading and multipath during implementation. Hence, the whole implementation is carried out in a RF cable environment.

The rest of this chapter is organized as follows. Section 4.2 describes the transmitter and receiver setup. Section 4.3 describes the implementation procedure and the summary is presented in section 4.4.

4.2 Implementation setup

The hardware setup is shown in figure 4.1. The following section explain the transmitter part of the setup.

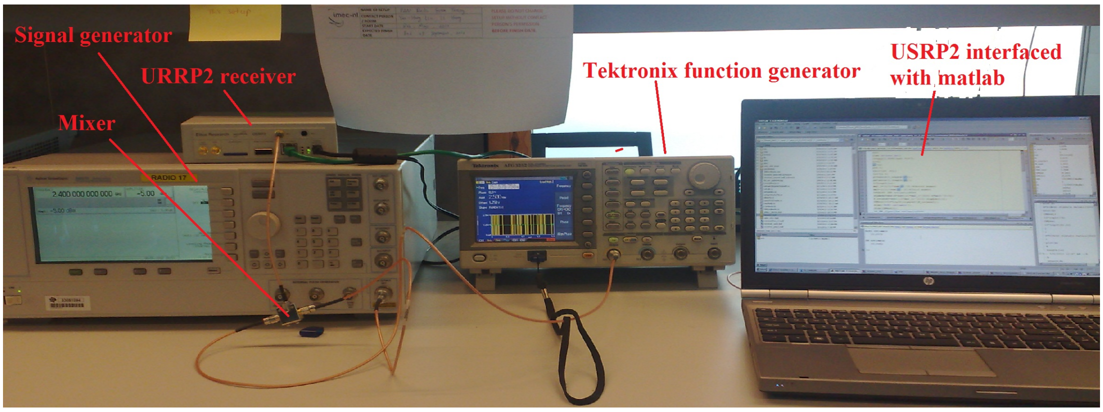

Figure 4.1: Implementation setup consisting of Tektronix function generator, Agilent signal generator, mixer, USRP2 receiver and the MATLAB interface

4.2.1 Transmitter setup

The transmitter part includes the Tektronix arbitrary/function generator, mixer and the Agilent signal generator. The functions of each of the modules are described below.

4.2.1.1 Tektronix arbitrary/function generator

Any arbitrary waveform can be generated by the Tektronix arbitrary/function generator. The software ArbExpress from Tektronix is used for this purpose. The procedure for OOK pulse generation is explained below.

- The OOK pulse is generated in MATLAB and saved as a *.tex file.
- The tex file can be loaded to the ArbExpress software which converts the data into the pulse form as shown in figure 4.2 that can be used in the function generator.

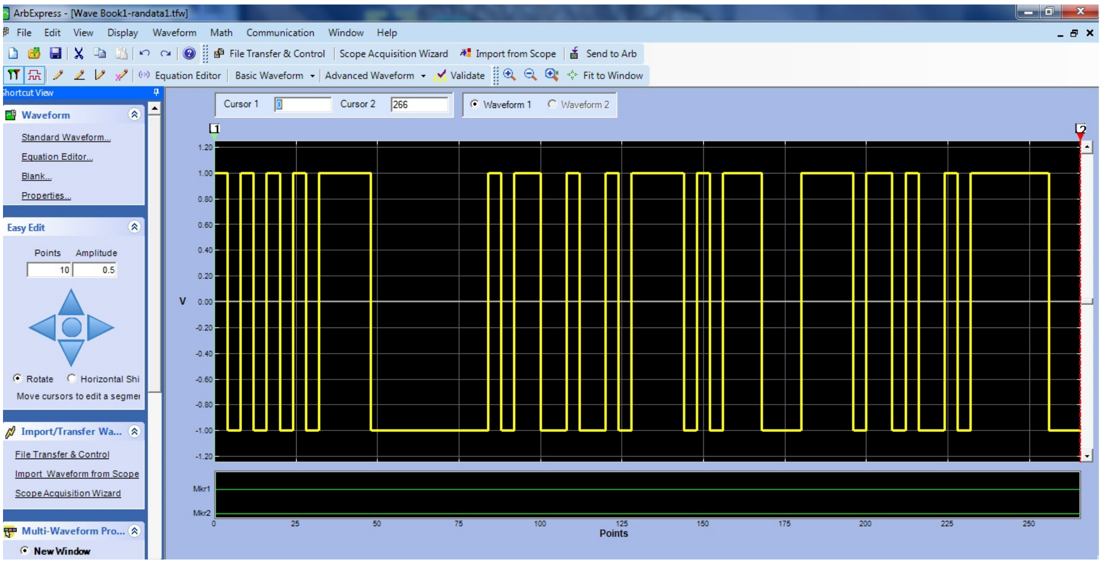

Figure 4.2: The OOK pulse waveform output from the ArbExpress tool

- The properties of the OOK signal such as the data rate can be adjusted in the function generator. We have set the data rate to be 50 kbps.
- The output of the function generator is given to one of the inputs of the mixer.

4.2.1.2 Agilent signal generator

The signal generator is used to generate the RF waveform at the centre frequency of 2.4 GHz. The spectrum of the generated signal is obtained from the spectrum analyzer and it is shown in figure 4.3. The RF output of the signal generator is given to the other input of the mixer.

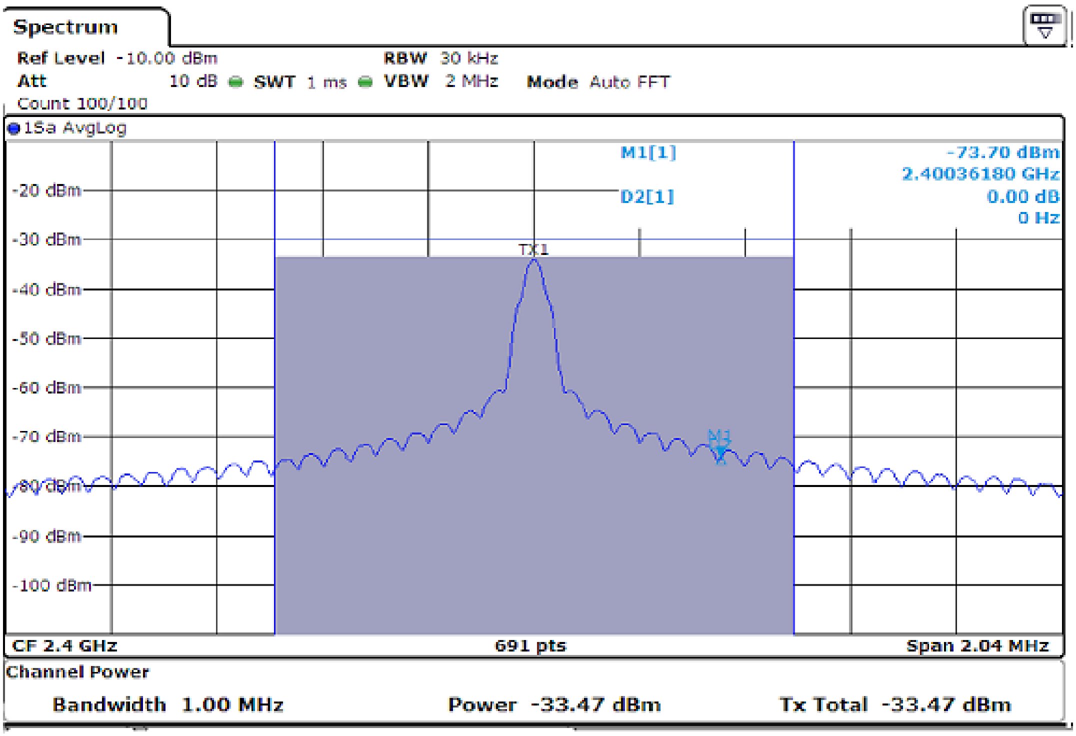

Figure 4.3: The power spectrum of the RF output of the signal generator at a centre frequency of 2.4 GHz is shown.

4.2.1.3 Mixer

The mixer is used to convert the transmitted baseband OOK pulse from the function generator to RF. It combines the two inputs from the signal generator and the function generator and gives the required RF signal at its output terminal. The output of the mixer is connected to the RF input of the USRP2 receiver.

In the following section, the receiver setup is discussed in detail.

4.2.2 Receiver setup

The USRP2 hardware and MATLAB interface are the components of the receiver setup. The functions of each of the components is described below.

4.2.2.1 USRP2 hardware

The USRP2 is a software defined radio platform developed by Ettus research, [20]. The USRP2 hardware used in this implementation has a RFX2400 daughter board which can operate in the range of 2.3-2.9 GHz. The USRP2 acts as a direct conversion receiver and the baseband processing is done in MATLAB. Figure 4.4 shows the simplified block diagram of USRP2. The received RF signal is down converted to baseband by the RFX2400 daughter boards. The analog signal is digitized by two 14 bit ADCs' operating at 100 mega samples per second (MS/s). The digitized complex baseband samples from the output of the ADCs' are then passed through a digital down converter

(DDC). The DDC acts as a decimating low pass filter. These samples are fed through a gigabit ethernet port to the MATLAB interface and the baseband processing is done in MATLAB. If the decimation is not done, the samples reach the gigabit ethernet port at the rate of 2800 MS/s, which the interface cannot handle. Therefore, a minimum decimation factor of 4 is assigned to the USRP2 device. Consequently, the USRP2 can support a maximum data rate of 25 Mbps. There are certain steps that have to be done to configure the USRP2 hardware. The detailed information can be found in [21].

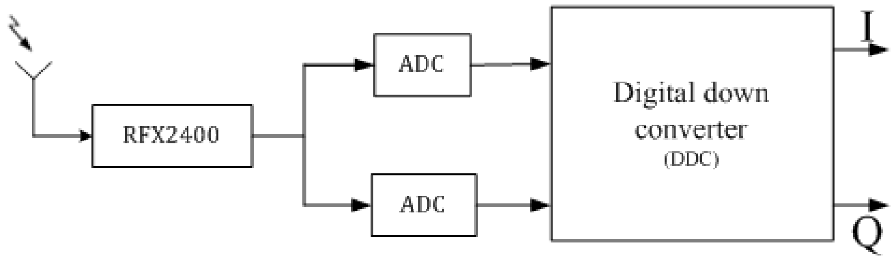

Figure 4.4: Block diagram of USRP2 device.

4.2.2.2 MATLAB interface

The baseband processing can be done in various platforms such as GNU Radio, MATLAB etc. In our case, the USRP2 is interfaced with MATLAB via the gigabit ethernet port interface. The tool box for interfacing MATLAB with the USRP2 must be installed and it is available in the MATLAB website, [22]. The simulink model is shown in figure 4.5. The sdru receiver block interface the USRP2 hardware with MATLAB.

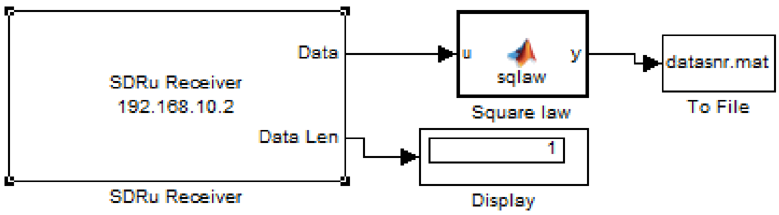

Figure 4.5: Simulink model of the USRP2 interface with the square law detection.

The parameters of the sdru receiver block are shown in figure 4.6. The centre frequency should be set to the desired frequency of interest. The LO offset can be adjusted if there is any inherent frequency offset in the local oscillator. The gain can be adjusted depending on the received signal level. The decimation factor is the most important parameter. The minimum value is 4 as described in section 4.2.2.1. The maximum value is 512. The decimation factor (F_d) is set based on the following formula.

$$F_d = \frac{S_r}{T_r \times U_f}, \tag{4.1}$$

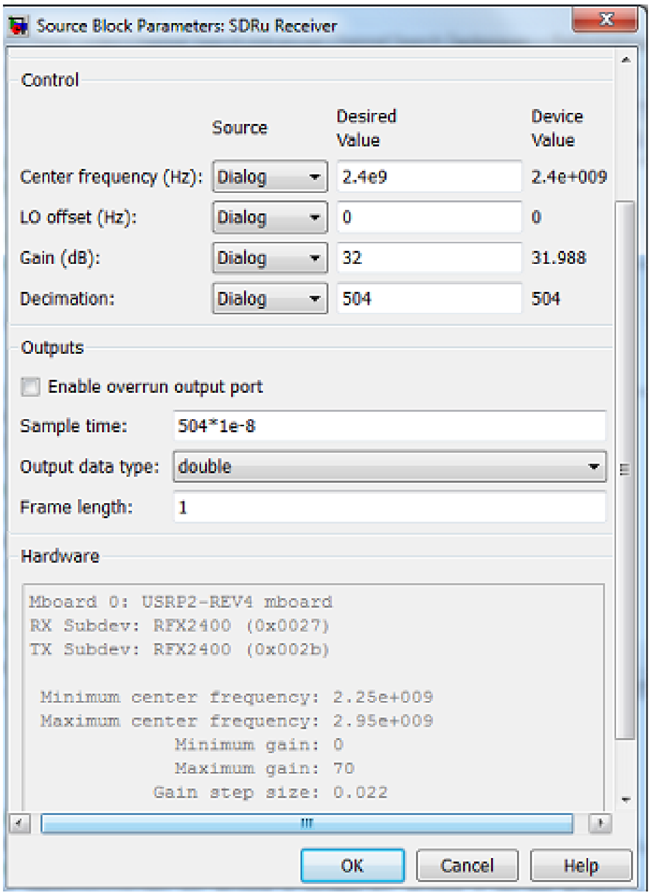

Figure 4.6: Parameters of the sdru receiver block.

where, S_r is the ADC sampling rate (100 MS/s), T_r is the transmitted bit rate and U_f is the required number of samples per bit duration,i.e., the oversampling factor. The sampling time is given by F_d/S_r. Output data type can be set to double if floating point precision is required. Frame length can be varied depending on requirements.

The complex baseband samples from the sdru block is fed to the square law detector. The square of the envelope of the complex baseband signal samples from the square law detector is stored and SNR estimation is done on the stored real time data samples. The real time data samples for SNR= 10 dB and SNR= 15 dB are shown in figure 4.7 and figure 4.8, respectively.

In the following section, the implementation procedure is discussed briefly.

4.3 Implementation procedure

The moments based M_2M_3 and expectation maximization (EM) NDA estimators are validated during the implementation. The implementation procedure is described below.

- At first, reference SNR is estimated at a specified transmit (Tx) power level.

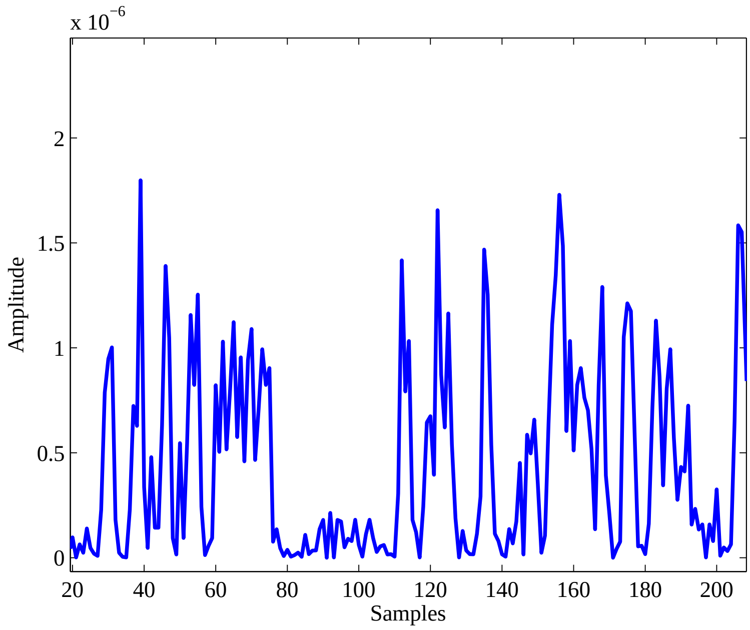

Figure 4.7: The real time data samples for $SNR = 10$ dB

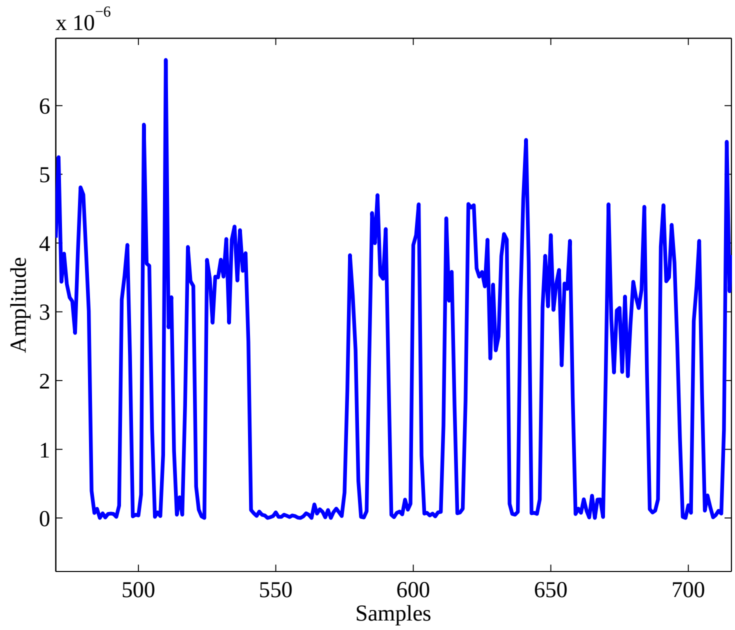

Figure 4.8: The real time data samples for $SNR = 15$ dB

- The Tx power is varied using the signal generator and the SNR is estimated again.
- The relative difference between the reference SNR and estimated SNR is found to be in accordance with the variation in the Tx power level.
- It is also verified that the EM estimates are larger than the moments based estimates at low SNR and the moments based estimates are not reliable at high SNR

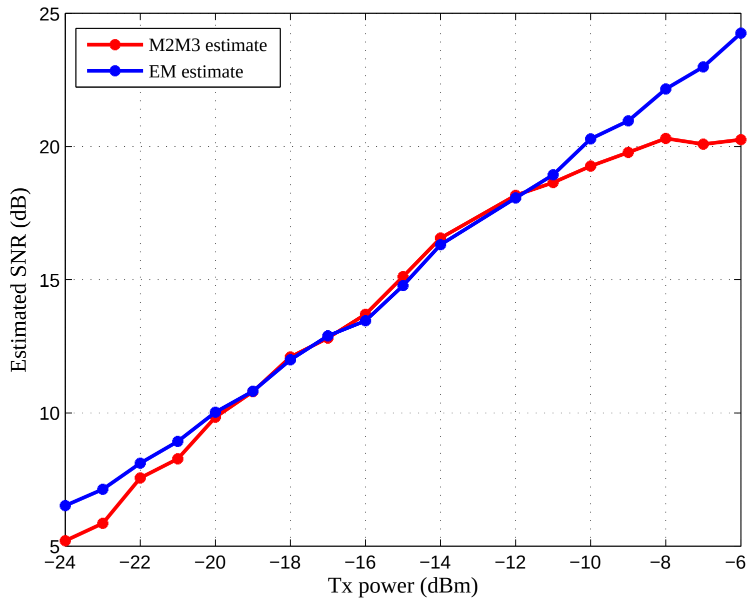

Figure 4.9: Estimated SNR against Tx power.

which is in accordance with the simulation results.

Figure 4.9 shows the plot of SNR estimates of $M_2M_3$and EM estimators plotted against the Tx power. It is evident that the EM estimates show a bias at low SNR region (SNR$<$ 10 dB). The EM and M_2M_3 estimates are close to each other in the region $10 \leq$ SNR ≤ 18 dB and the moments based estimates are not reliable for SNR$>$ 18 dB.

4.4 Summary

In this chapter, the implementation of the proposed NDA M_2M_3 and EM SNR estimators in the USRP2 platform is described in detail. The transmitter and receiver blocks are explained in detail and the procedure to setup the hardware is also clearly explained. The implementation procedure is described and the results of the SNR estimates with the real time data are shown. It is found that the EM estimates show a bias at low SNR region (SNR$<$ 10 dB). The EM and M_2M_3 estimates are close to each other in the region $10 \leq$ SNR ≤ 18 dB and the M_2M_3 estimates are not reliable for SNR$>$ 18 dB.

Conclusions and future scope 5

5.1 Conclusions

In this thesis, we addressed the problem of interference mitigation in the low power non-coherent on-off keying (OOK) receiver based wakeup radio. The main contributions of this thesis are,

- Normalized max-zero likelihood (NML) method for non-coherent detection of OOK signals.
- Data aided (DA) and non data aided (NDA) signal to noise ratio (SNR) estimation techniques for non-coherent OOK receivers.
- Threshold based and maximum-a-posteriori (MAP) detector based interference mitigation techniques for continuous wave (CW) and OOK modulated interferers.
- Implementation of NDA SNR estimation techniques in the universal software radio peripheral 2 (USRP2) platform.

5.1.1 NML method

NML method is proposed for non-coherent detection of OOK signals. It is shown that the NML detection improves the bit error rate (BER) performance and there is a gain of 1 dB at BER of 2×10^{-4} for $\alpha = 0.3$ when compared to maximum likelihood (ML) detection method for the wakeup radio architecture. It is also shown that the NML gain decreases as α increases.

5.1.2 SNR estimation

Non-coherent detection of OOK signals requires the knowledge of SNR. Therefore, DA and NDA SNR estimation techniques are proposed for non-coherent OOK receivers. ML and M_1V estimators are proposed for DA SNR estimation and the Cramer-Rao lower bound (CRLB) is derived for DA estimation. It is shown that ML estimator is biased at low SNR and the performance of both the DA estimators are similar for SNR$>$ 8 dB. M_1M_2, M_2M_3 and expectation maximization (EM) estimators are proposed for NDA SNR estimation. It is shown that M_1M_2 estimator is not suitable for equiprobable symbol conditions and M_2M_3 estimator overcomes this problem. It is also shown that the moments based NDA estimators are unreliable at high SNR and EM estimator is biased at low SNR. Hence, hybrid $M_2M_3 - EM$ and $M_1M_2 - EM$ estimators are proposed to overcome the limitations. The bit error rate (BER) performance for each of these estimators is simulated and found to be in agreement with the theoretical BER.

5.1.3 Interference mitigation

The SNR estimation techniques are extended for interference mitigation. CW and OOK modulated interferers are considered in this thesis. DA estimation techniques are used to estimate the interference, signal and noise power in the case of CW interferers. NDA estimation techniques can be used in the case of OOK modulated interferers. The decision threshold and MAP detector based techniques are proposed for interference mitigation. In the case of CW interferer, it is shown that both the techniques perform similarly and there is a gain of 1 dB at 2.5×10^{-2} BER when compared to the without interference case. It is shown for OOK modulated interferer that the threshold based technique is suitable for $C/I > 0$ dB and the MAP detector based technique is suitable for both $C/I \geq 0$ dB and $C/I < 0$ dB. It is also shown the both the techniques perform similarly for $C/I > 0$ dB. The extension of MAP detection to joint detection of both the desired and interfering signal is proposed in the case of OOK modulated interferer. Though the proposed interference mitigation techniques are not fool proof, they are suitable to mitigate the interference in the specified C/I ranges and also effectively mitigate the interference which are much greater than the desired signal level ($C/I \ll 0$ dB). This is an important result in the case of low power wakeup radio, as the chance of interfering signal to be much greater than the desired signal is high.

5.1.4 Implementation of NDA SNR estimation

The implementation of the proposed NDA M_2M_3 and EM SNR estimators in the USRP2 platform is discussed in detail. Important issues in the configuration of the setup are also discussed. The implementation procedure is described and the results of the SNR estimates with the real time data are shown. It is found that the EM estimates show a bias at low SNR region (SNR$<$ 10 dB). It is also shown that the EM and M_2M_3 estimates are close to each other in the region $10 \leq \text{SNR} \leq 18$ dB and the M_2M_3 estimates are not reliable for SNR$>$ 18 dB.

In the following section, we give a few suggestions for future research.

5.2 Suggestions for future research

- The NML detection method can be extended to M-ary frequency shift keying (MFSK) receivers as they are similar to OOK but operate at multiple tones.
- It is difficult to obtain a closed form expression for the CRLB in the case of NDA SNR estimation. Hence, theoretical study on the numerical evaluation of CRLB for NDA SNR estimation can be carried out in future.
- The interference mitigation techniques are proposed for the case of OOK modulated, CW and modulated interferers with constant modulus. The extension of these techniques for the case of non constant modulus interferes such as MQAM and MPAM can be studied in future.
- We had considered only AWGN channel in this thesis. Extension of the proposed techniques for the case of fading channels provides a huge scope of further research.

- In this thesis, we implemented NDA SNR estimation techniques in the USRP2 platform. In future, the implementation of the proposed interference mitigation techniques can be done in the USRP2 platform.

Publications

1. V.Sridharan, N. F. Kiyani and H. Nikookar, "SNR estimation and interference mitigation techniques for non-coherent detection of OOK signals", in *Proc. WIC/IEEE Symp. on Inf. theory and Signal proc.*, May, 2012.

2. V.Sridharan, N. F. Kiyani, H. Nikookar and G. Dolmans, "Non data aided SNR estimation for non-coherent OOK receivers", (submitted) in *Proc. IEEE Globecom Wireless Comm. Symp.*, Dec., 2012.

3. V. Sridharan, N. F. Kiyani and H. Nikookar, "Normalized max-zero likelihood detection of on-off keying signals", To be submitted to *IEEE Wireless Comm. Letter*, 2012.

4. V. Sridharan, N. F. Kiyani and H. Nikookar, "Interference mitigation techniques for non-coherent OOK receivers in the presence of OOK modulated interferers", To be submitted to *IEEE WCNC* or *VTC* or *ICC*, 2013.

Bibliography

[1] N. F. Kiyani, Y. Zhang, P. Harpe, X. Huang and G. Dolmans, "Performance analysis and measurement results of an ultra low power wakeup radio in the presence of interference", *IEEE URSI General Assembly and Scientific Symposium of Int. Union of Radio Science*, Aug., 2011.

[2] N. F. Kiyani, P. Harpe and G. Dolmans, "Performance analysis of OOK modulated signals in the presence of ADC quantization noise", in *Proc. IEEE VTC*, May, 2012.

[3] M. Schwartz, W. Bennett, and S. Stein, *Communication systems and techniques.* New York: McGraw-Hill, 1966.

[4] J. Proakis, *Digital Communications*, 5th ed. McGraw-Hill, 2007.

[5] http://ens.ewi.tudelft.nl/Education/courses/et4147/sheets/*beam_leus*.pdf

[6] http://ens.ewi.tudelft.nl/Education/courses/et4147/sheets/adaptive_leus.pdf

[7] J. F. Cardoso and A. Souloumiac , "Blind beamforming for non-Gaussian signals," in *Proc. IEE Radar and signal processing,* vol. 140, no. 6, pp. 362-370, Dec., 1993.

[8] P. Patel and J. Holtzman, "Analysis of a simple successive interference cancellation scheme in a DS/CDMA system," *IEEE Journ. Select. Areas. Commun.,* vol. 12, pp. 796 807, June, 1994.

[9] D. Divsalar and M. K. Simon, "Improved CDMA performance using parallel interference cancellation," *JPL Publication,* pp. 95 -21, Oct. 1995.

[10] S. B. Hoeher, P. A. Hoher and W. Xu,"Single antenna interference cancellation for cellular TDMA networks by means of decoupled linear filtering/nonlinear detection," in *Proc. IEEE PIMRC,* pp. 1-5, 11-14, Sept., 2006.

[11] P. A. Hoeher, S. B. Hoeher, S. Deng, C. Krakowski and W. Xu, "Single antenna interference cancellation (SAIC) for cellular TDMA networks by means of joint delayed-decision feedback sequence estimation," *IEEE Trans. Wireless Comm.*, vol. 5, no. 6, pp. 1234-1237, June, 2006.

[12] I. Trachanas and N. Fliege, "A novel phase based SNR estimation method for constant modulus constellations," in *Proc. ISCCSP Int. Symposium*, pp. 1179 - 1183, March, 2008.

[13] D. Pauluzzi and N. Beaulieu, "A comparison of SNR estimation techniques for the AWGN channel," *IEEE Trans. Commun.*, vol. 48, no. 10, pp. 1681 -1691, Oct., 2000.

[14] P. Gao and C. Tepedelenlioglu, "SNR estimation for non-constant modulus constellations," in *Proc. IEEE WCNC*, vol. 1, pp. 24 -29, March, 2004.

[15] W. Gappmair, R. Lopez-Valcarce, and C. Mosquera, "Cramer-Rao lower bound and EM algorithm for envelope-based SNR estimation of nonconstant modulus constellations," *IEEE Trans. Commun.*, vol. 57, no. 6, pp. 1622 -1627, June, 2009.

[16] S. Hassan and M. Ingram, "SNR estimation for a non-coherent M-FSK receiver in a slow flat fading environment," in *Proc. IEEE Int. Conf.*, pp. 1 -5, May, 2010.

[17] Q. Tang, S. K. S. Gupta and L. Schwiebert, "BER performance analysis of an on-off keying based minimum energy coding for energy constrained wireless sensor applications," in *Proc. ICC*, vol. 4, pp. 2734 -2738, May, 2005.

[18] S. Kay, *Fundamentals of Statistical Signal Processing:Estimation Theory*. New Jersey: Prentice Hall, 1993.

[19] T. Moon, "The Expectation-Maximization algorithm," *IEEE Signal Processing Magazine*, vol. 13, no. 6, pp. 47 -60, Nov., 1996.

[20] https://www.ettus.com/product

[21] http://files.ettus.com/*uhd_docs*/manual/html

[22] http://www.mathworks.nl/discovery/sdr/usrp.html